Politechnika Warszawska

WYDZIAŁ MECHATRONIKI

Praca dyplomowa inżynierska

na kierunku Mechatronika
w specjalności Urządzenia i systemy mechatroniczne

CFD Analysis of a Ventricular Assist Device

numer pracy według wydziałowej ewidencji prac: 114C-ISA-MT/302601/1258160

Harshit Verma

numer albumu 302601

promotor
dr inż. Adam Piechna

konsultacje

WARSZAWA 2025

1 Contents

2 Abstract

2.1 English Version

CFD analysis of a Ventricular Assist Device

This thesis presents a Computational Fluid Dynamics (CFD) analysis of a hydraulically representative model of the HeartMate 3 ventricular assist device (VAD). Motivated by the global burden of heart failure and the limitations of current VADs, the study aims to replicate and optimize flow dynamics and device efficiency through virtual prototyping. Using ANSYS Fluent, the research models blood flow through a simplified centrifugal pump geometry inspired by HeartMate 3, evaluating performance across multiple RPMs and outlet pressures using both SST k-ω and RNG k-ε turbulence models. Key metrics such as pressure head, mass flow rate, hydraulic and mechanical power, and efficiency are computed. A modified impeller blade design is also assessed to examine its impact on flow characteristics and wall shear stress. Results demonstrate strong agreement with published HeartMate 3 pump data at high flow conditions, with SST k-ω showing better stability and near-wall resolution. The study identifies Best Efficiency Points (BEPs) for each RPM and confirms expected centrifugal pump behavior, while highlighting design trade-offs in blade modifications. Limitations related to geometry simplification, steady-state assumptions, and Newtonian fluid modeling are acknowledged. Overall, this CFD model offers a validated foundation for future VAD design improvements and hemocompatibility studies.

2.2 Polish Version

Analiza CFD urządzenia wspomagającego pracę komór serca

Niniejsza rozprawa przedstawia analizę obliczeniowej dynamiki płynów (CFD) hydraulicznie reprezentatywnego modelu urządzenia wspomagającego pracę komór HeartMate 3 (VAD). Motywowane globalnym obciążeniem niewydolnością serca i ograniczeniami obecnych VAD, badanie ma na celu odtworzenie i optymalizację dynamiki przepływu i wydajności urządzenia poprzez wirtualne prototypowanie. Korzystając z programu ANSYS Fluent, w badaniu modelowano przepływ krwi przez uproszczoną geometrię pompy odśrodkowej inspirowaną HeartMate 3, oceniając wydajność przy wielu obrotach i ciśnieniach wylotowych przy użyciu modeli turbulencji SST k-ω i RNG k-ε. Obliczono kluczowe wskaźniki, takie jak wysokość podnoszenia, masowe natężenie przepływu, moc hydrauliczna i mechaniczna oraz sprawność. Zmodyfikowana konstrukcja łopatek wirnika jest również oceniana w celu zbadania jej wpływu na charakterystykę przepływu i naprężenie ścinające ściany. Wyniki wykazują silną zgodność z opublikowanymi danymi pompy HeartMate 3 w warunkach wysokiego przepływu, przy czym SST k-ω wykazuje lepszą stabilność i rozdzielczość przyścienną. Badanie identyfikuje punkty najlepszej wydajności (BEP) dla każdego RPM i potwierdza oczekiwane zachowanie pompy odśrodkowej, jednocześnie podkreślając kompromisy projektowe w modyfikacjach łopatek. Uznano ograniczenia związane z uproszczeniem geometrii, założeniami stanu ustalonego i modelowaniem płynu newtonowskiego. Ogólnie rzecz biorąc, ten model CFD stanowi zweryfikowaną podstawę dla przyszłych ulepszeń projektowych VAD i badań hemokompatybilności.

2.3 Hindi Version

वेंट्रिकुलर असिस्ट डिवाइस का CFD विश्लेषण

यह थीसिस हार्टमेट 3 वेंट्रिकुलर असिस्ट डिवाइस (VAD) के हाइड्रॉलिक रूप से प्रतिनिधि मॉडल का कम्प्यूटेशनल फ्लुइड डायनेमिक्स (CFD) विश्लेषण प्रस्तुत करती है। हृदय विफलता के वैश्विक बोझ और वर्तमान VAD की सीमाओं से प्रेरित होकर, अध्ययन का उद्देश्य वर्चुअल प्रोटोटाइपिंग के माध्यम से प्रवाह गतिशीलता और डिवाइस दक्षता को दोहराना और अनुकूलित करना है। ANSYS फ्लुएंट का उपयोग करते हुए, अनुसंधान हार्टमेट 3 से प्रेरित एक सरलीकृत केन्द्रापसारक पंप ज्यामिति के माध्यम से रक्त प्रवाह को मॉडल करता है, SST k-ω और RNG k-ε टर्बुलेंस मॉडल दोनों का उपयोग करके कई RPM और आउटलेट दबावों में प्रदर्शन का मूल्यांकन करता है। दबाव सिर, द्रव्यमान प्रवाह दर, हाइड्रोलिक और यांत्रिक शक्ति, और दक्षता जैसे प्रमुख मीट्रिक की गणना की जाती है। प्रवाह विशेषताओं और दीवार कतरनी तनाव पर इसके प्रभाव की जांच करने के लिए एक संशोधित प्ररित करनेवाला ब्लेड डिजाइन का भी मूल्यांकन किया जाता है। परिणाम उच्च प्रवाह स्थितियों में प्रकाशित हार्टमेट 3 पंप डेटा के साथ मजबूत समझौते को प्रदर्शित करते हैं, जिसमें SST k-ω बेहतर स्थिरता और निकट-दीवार रिज़ॉल्यूशन दिखाते हैं। अध्ययन प्रत्येक RPM के लिए सर्वश्रेष्ठ दक्षता बिंदुओं (BEP) की पहचान करता है और अपेक्षित केन्द्रापसारक पंप व्यवहार की पुष्टि करता है, जबकि ब्लेड संशोधनों में डिज़ाइन ट्रेड-ऑफ़ को उजागर करता है। ज्यामिति सरलीकरण, स्थिर-अवस्था मान्यताओं और न्यूटोनियन द्रव मॉडलिंग से संबंधित सीमाओं को स्वीकार किया जाता है। कुल मिलाकर, यह CFD मॉडल भविष्य के VAD डिज़ाइन सुधारों और हेमोकम्पैटिबिलिटी अध्ययनों के लिए एक मान्य आधार प्रदान करता है।

3 Introduction

3.1 Background and Motivation

In recent years, there has been an increase in cardiovascular diseases around the world. Among them the most prominent being heart failure. According to the World Health Organization (WHO), over 64 million people suffer from heart failure worldwide, contributing to millions of hospitalizations and significant mortality annually. In the United States alone, nearly 6.5 million adults live with heart failure, with the prevalence projected to increase by 46% by 2030 [22].

The increase is primarily driven by an aging population, lifestyle-related risk factors such as hypertension, diabetes, and obesity, and the improved survival rates from myocardial infarctions and other cardiac diseases. These factors collectively place a massive strain on healthcare systems and underscore the critical need for advanced treatment options beyond pharmacological therapy and surgical revascularization.

Among these advanced options, ventricular assist devices (VADs) have emerged as life-saving tools for patients with end-stage heart failure. VADs serve not only as a bridge to transplantation but also as destination therapy for patients who are not transplant candidates. In recent decades, technological advancements in VADs have led to significant improvements in patient survival, quality of life, and device durability.

The evolution from bulky, pulsatile devices to compact, continuous-flow systems has transformed the landscape of mechanical circulatory support [23]. Earlier devices like HeartMate 2 were usually bulkier and were not considered a good long-term solution. (Figure 2) Third-generation VADs, such as HeartMate 3, have introduced fully magnetically levitated impellers that virtually eliminate mechanical contact, thereby reducing wear, thrombosis, and hemolysis. The shift from mechanical to magnetic levitation has also allowed for smoother flow paths and more physiologically relevant circulatory dynamics.

3.2 Literature Review

3.2.1 Evolution of Ventricular Assist Devices (VADs)

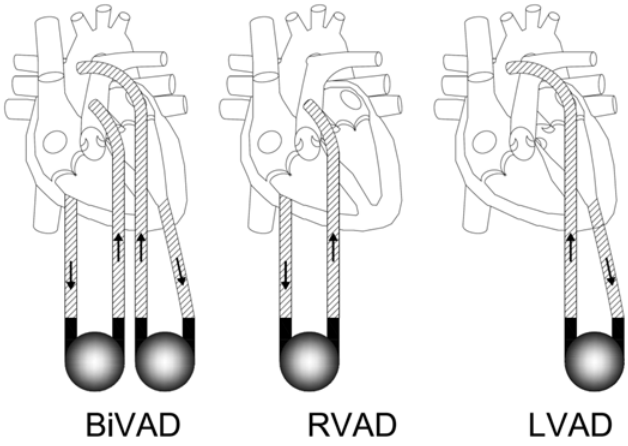

Figure 1. Types of VADs based on Chambers supported. [2]

Heart transplants remain inacessible to many patients due to organ shortages or indivisual medical conditions. Ventricular Assist Devices (VADs) serve as critical alternatives, functioning as mechanical pumps that augment or replace the heart's pumping ability. VADs include Left Ventricual Assist Devices (LVADs), Right Ventricular Assist Devices (RVADs), and Bi-Ventricular Assist Devices (Bi-VADs)(Figure 1). These devices are implanted either between the left atrium and descending aorta or between the right atrium ans pulomonary artery. The development of Ventricular Assist Devices (VADs) has spanned multiple decades, evolving through three dinstinct genrations.

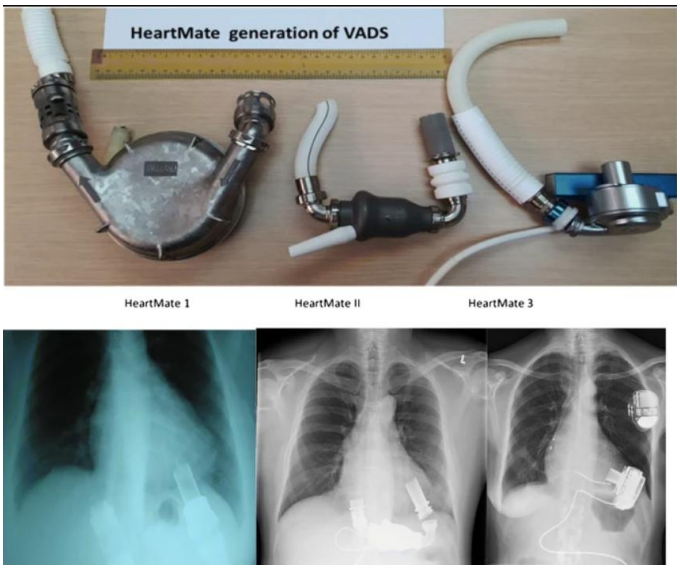

Figure 2. Three generations of heartmate 3. [53]

The first-generation VADs were primarliy pulsatile, designed to mimic the natural heartbeat. These devices used mechanical diaphragms or pusher plates to generate a

stroke volume and required large external driver consoles. While they provided a phsyiological form of blood flow, they suffered from severe limitations such as large size, noise low durabiliyt, and mechanical complexity[27]. The clinical utitlity of these devices was further restricted due to the high incidence of infections and thromboembolic complications, prompting a need for more efficient and reliabel solutions [3]. This led to the second-genration VADs, which introduced continous acial flow mechanisms. These pumps were smaller, simpler and more durable because they contained fewer moving parts and eliminated pulsatility requirement. By spinning a rotor at high speeds (ofter>10,000 RPM), these devices could provide sufficient flow with relatively compact designs. The HeartMate 2 (Figure 2), for example, demonstrated imroved survival and reduced mechanical failure compared to its pulsatile predecessors [28]. However, the absence of pulsatility raised concerns abut adverse vascular effect and gastrointestinal bleeding. Addtionally, the high-speed rotors intrduced high shear enviroments, contributing to hemolysis and acquired von Williebrand syndrome. The advent of third-generation VADs marked a significant shift in VAD technology. These centrifugal flow devices use magnetic or hydrodynamic levitation to suspend the rotor withing the pump housing, effctively elminiating mechanical contact and wearv [7]. The HeartMate 3 represents the clinical standard of this generaton. Its magnetically levitated rotor, wide flow gaps, intrinsic artifical pulse mode helps minimize hemolysis and thrombosis while improving pump longetivity [26][29]. The MOMNETUM 3 trial confirmed superior outomes for HeartMate 3 over seconf genration HeartMate 2 in terms of freedom from diabling strke, pump thrombosis, and need for reparation [26].

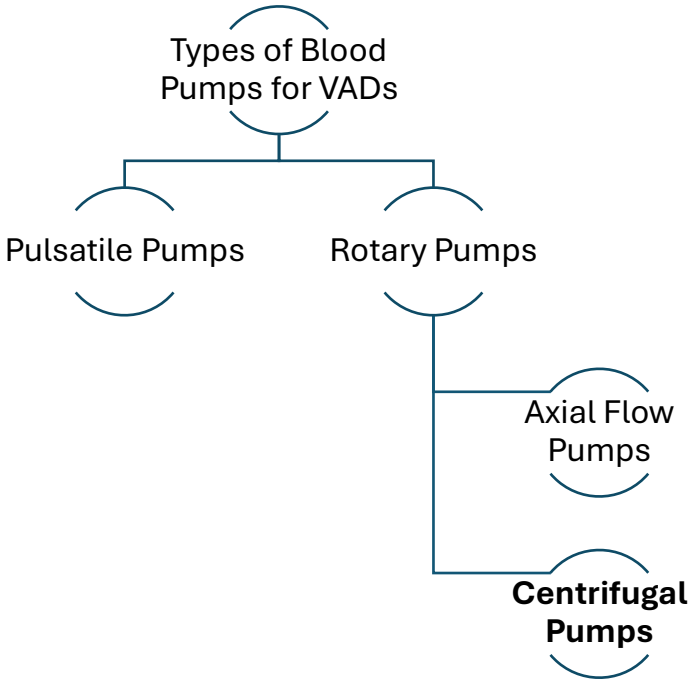

Figure 3. Flow chart explaining the generations of blood flow pumps used as VADs [10].

VADs utilize two primary blood pumps Rotary Continuous Flow Pumps and Positive Displacement Pulsatile Pumps (Figure 3) [10].

1. Pulsatile Pumps:

These pumps mimic the heart's natural pulsatile flow. Blood flows via inlet and outlet valves, creating jets that generate vortices to wash the pump chamber. While wall shear stresses are low, jets introduce high shear rates.

2. Rotary Pumps:

These pumps operate in rotary motion, with two subcategories:

1. Centrifugal pumps: These pumps use centrifugal force to direct blood towards the blade's edges, creating high pressure near lower flow rates.
2. Axial Flow Pumps: Push blood parallel to the pumps axis, generating higher flow rates but requiring faster rotational speeds. Their smaller size and tubular design make them easier to implant.

3.2.2 CFD as a tool in Biomedical Device Development

Computational Fluid Dynamics (CFD) uses numerical methods to approximate the equations governing fluid motion. Computational Fluid Dynamics (CFD) has become indispensable in the field of biomedical engineering, particularly for simulating blood flow through complex geometries such as heart valves, stents, and ventricular assist devices. Unlike experimental methods, CFD allows for non-invasive, cost-effective, and highly detailed analysis of internal flow behavior, making it ideal for early-stage device design and optimization [30].

The Navier-Stokes equations, which govern fluid motion, are numerically solved using methods like Finite Volume Method (FVM) in solvers such as ANSYS Fluent. These simulations provide insights into pressure distributions, velocity profiles, shear stress, and turbulence intensity. In rotary blood pumps, CFD has been used to investigate the impact of blade design, volute geometry, and boundary conditions on pump performance and blood damage [31]. Studies have also demonstrated the capability of CFD to predict Wall Shear Stress (WSS), a key factor in evaluating blood damage and thrombus formation potential [32].

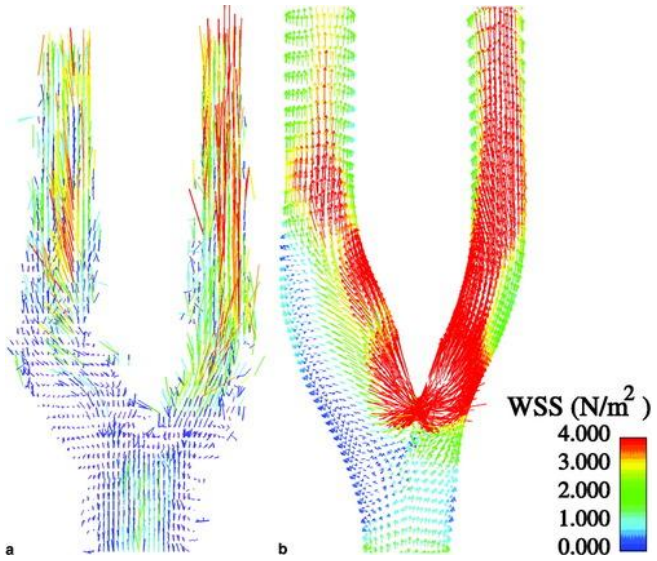

Figure 4. Comparison of MRI and CFD simulations for WSS.[54]

Multiple researchers have validated the use of CFD against in vitro and in vivo experimental data. For instance, Papathanasopoulou et al. demonstrated (Figure 4) the accuracy of CFD predictions by comparing time-resolved wall shear stress vectors in a carotid bifurcation model with measurements obtained from Magnetic Resonance Imaging (MRI) [54]. Similarly, Garon and Farinas evaluated Wall Shear Stress (WSS) in artificial organs, demonstrating that CFD predictions closely matched experimental shear data, especially in high-shear regions [32].

CFD studies are also instrumental in optimizing blade designs, particularly the blade count, curvature, thickness, and tip clearance. These parameters critically influence flow recirculation and stagnation zones which are directly linked to hemolysis and thromboembolism risk. Optimization through CFD allows for rapid testing of geometrical variations without physical prototyping, drastically reducing development cycles.

Computational Fluid Dynamics (CFD) has become an indispensable tool in the analysis and optimization of centrifugal pump performance. The review by Jaiswal [5] provides a comprehensive overview of how CFD techniques are applied to model the flow inside pumps, helping identify areas for efficiency improvement and performance enhancement.

CFD modeling allows detailed visualization of internal flow characteristics, including velocity vectors, pressure distribution, turbulence intensity, and regions of flow separation or recirculation. These insights enable engineers to diagnose performance losses that are otherwise difficult to detect through experimental methods.

Jaiswal [5] emphasizes that key efficiency impacting factors, such as blade geometry, impellers-diffuser spacing and volute design, aca be systematically studies using CFD simulations. By varying design parameters virtually and analyzing their impact on flow

behavior and pump head, researchers can iterate toward optimized geometries before physical prototyping.

Among the simulation techniques discussed, the use of turbulence models like k-ε and k-ω is common, though the accuracy of these models can vary based on the pump type and Reynolds number. Moreover, the use of structured or unstructured meshing strategies affects the precision of the results, especially near complex blade surfaces or tight clearances in the impeller.

In terms of performance metrics, Head, Flow Rate, Hydraulic Efficiency, and Net Positive Suction head (NPSH) are among the most analyzed outputs in CFD pump studies. The highlights that CFD based optimization typically leads to efficiency improvements in the range of 3-7%, depending on the pump design and simulation accuracy.

In the context of Ventricular assist Devices (VADs) like HeartMate 3, these methods are directly applicable. The small size and high-speed nature of rotary blood pumps introduce unique flow challenges, such as shear induced blood damage and hemolysis, which can also be evaluated via CFD using specialized non-Newtonian blood models and hemolysis prediction algorithms.

Thus, CFD modelling provides both a theoretical and practical foundation for improving VAD efficiency, particularly in centrifugal designs like HeartMate 3. This forms a key step toward enhancing clinical outcomes and reducing the physical burden on patients through more efficient, compact and durable devices,

Furthermore, CFD models can identify problematic zones such as low-velocity regions, high shear stress areas and regions of recirculation, which are common causes of thrombosis and hemolysis in VADs. Design modifications driven by sch insights have led to measurable improvements in both hydraulic performance and blood compatibility.

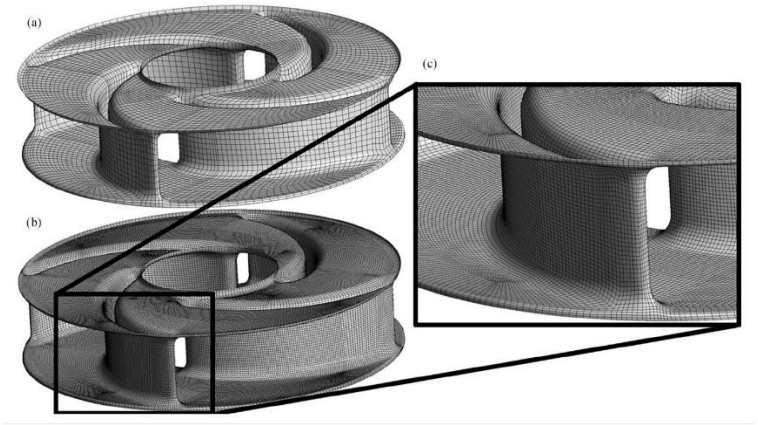

Figure 5. Rotary blades of Heartmate 3 with a fine mesh [1]

The use of accurate cardiovascular interaction models, as demonstrated in Crone et al. [1], is particularly relevant for centrifugal devices like the HeartMate 3, where performance depends heavily on both mechanical design (Figure 5) and adaptive flow regulation. Such designs centered simulation represent a pivotal shift in VAD development from static to intelligent, physiology-aware modelling.

3.2.3 Blood Rheology in CFD modelling

Blood, unlike most industrial fluid, exhibits non-Newtonian shear-thinning behavior, meaning its apparent viscosity decreases with increasing shear rate. This is due to its composition: a suspension of deformable red blood cells (RBCs), platelets, and plasma proteins. In large arteries or high-shear environments such as inside a rotary pump impeller, blood can be reasonably approximated as a Newtonian fluid due to the dominance of internal forces. However, in regions of low shear, such as recirculation zones or near-wall stagnation regions, the non-Newtonian nature of blood becomes critical to capture accurately [35].

Several models exist to represent blood's viscosity in CFD simulations. The Carreau-Yasuda model is widely regarded as the most accurate for physiological flows. It provides a smooth transition between the Newtonian plateau at high shear rates and power-law region at low shear rates[36]. The model is defined as:

$$\eta(\gamma') = \eta_\infty + (\eta_0 - \eta_\infty)[1 + (\lambda\gamma')^a]^{[(n-1)/a]}$$

where

- η is the viscosity [kg/m*s]
- γ̇ is the shear rate [s^-1]
- η_0 and η_∞ are the zero-shear and infinite-shear viscosities [Pa*s]
- λ is the time constant [Pa*s]
- a and n are model constants [s]

Another commonly used model is the Power-Law model, which is simpler but less accurate in transitional shear regions. Although this thesis adopts a Newtonian approximation for computational efficiency, future simulations are planned to integrate non-Newtonian models for improved WSS prediction.

Studies by Giersiepen at al. and Paul et al. have shown that under-predicting viscosity in low-shear regions can result in significant misrepresentation of blood damage risk [37]. In pup simulations, especially when investigating hemolysis platelet activation, the fidelity of blood rheology becomes even more important. Hence while the Newtonian model may suffice for pressure-flow characterization, it is insufficient for hemocompatibility studies, which is a limitation acknowledge in this work and addressed in future research directions.

3.2.4 Turbulence Modeling in Rotary Blood Pumps

In devices like the HeartMate 3, flow rates often exceed 5-10 L/min with small diameters and rotating machinery, resulting in Reynolds numbers ranging from 5,000 to 50,000, well into the turbulent regime. Accurately capturing this turbulence is essential to ensure that CFD predictions match real world pressure, velocity and shear profiles.

Most CFD studies employ Reynolds-Averaged Navier-Stokes (RANS) turbulence models due to their balance between computational efficiency and accuracy. The most relevant models include:

- SST k-ω model: Combines the robust near-wall resolution of the standard k-ω model with the free stream accuracy of the k-ε model. It is especially effective in predicting separation and wall bounded turbulence. It is the default choice for internal pump flows [38].
- RNG k-ε model: Derived using statistical methods from the Navier-Stokes equations, it is better suited for swirling and free-shear flows. It has been effectively used in many biomedical applications but is less accurate near walls.

Comparative studies, such as those by Boughner et al. and Zhang et al., have shown that the choice of turbulence model significantly affects predictions of recirculation zones, pressure drop, and WSS [39][40]. Therefore, this study incorporates all three models to evaluate their perspective performance in simulating the HeartMate 3 inspired geometry. Differences in predicted flow structures, pressure curves, mass flow rates will be critically analyzed to select the most accurate turbulence model for performance curve generation.

3.2.5 Existing CFD Studies on HeartMate and Similar Pumps

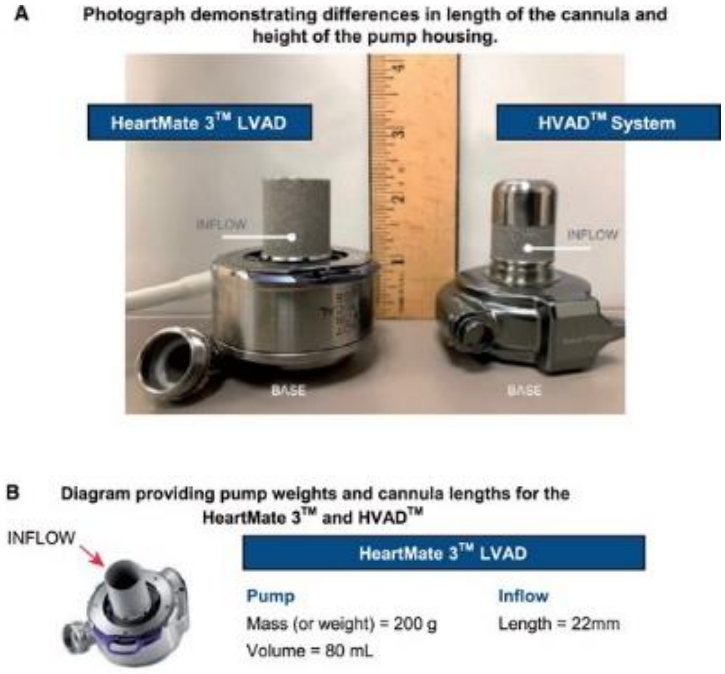

Figure 6. HeartMate 3 study showcases some dimensions measured in a study. [9]

Due to the proprietary nature of the HeartMate 3's internal geometry, the most published CFD research avoids direct replication of its design. However, many researchers have instead modeled functionality analogous rotary blood pumps to investigate hydraulic behavior, flow-induced stresses, and overall performance (Figure 6).

Fraser et al. [3] performed one of the earliest significant CFD studies on generic centrifugal rotary blood pumps, optimizing blade angle and analyzing flow separation ensuing the SST k-ω model. Wu et al. [29] validated CFD results of simplified LVAD models against in vitro experimental data, focusing on shear stress distributions and pressure profiles which are critical for predicting hemolysis.

Islam et al. and Sharma et al. [41][42] introduced parametric optimization techniques using 3d printed impellers and simplified centrifugal geometries, mimicking HeartMate like configuration. Their simulations demonstrated that increasing RPM improved pressure head but led to higher shear regions. They emphasized the role of flow path redesigns in shifting the Best Efficiency Point (BEP).

Recent studies by Crone et al. [1] and Zawawi et al. [13] also applied CFD and VAD simulations with increasing emphasis on system level integration and accurate physiological boundary conditions. Crone et al. specifically highlighted the use of dynamic boundary conditions and coupling with cardiovascular system models to more realistically simulate pump behavior across cardiac cycles.

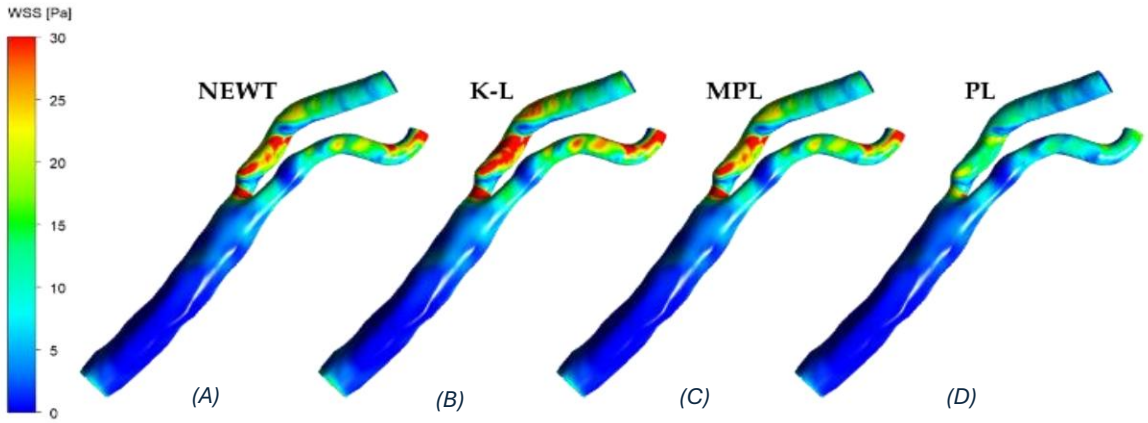

Figure 7. WSS on different Blood rheological models (A)Newtonian (B)K-L(C)Modified Power-Law(D)Power-Law, Newtonian model shows similar outputs when comparing hydraulic properties.

While these studies underscore the feasibility and effectiveness of CFD in blood pumping modeling, notable limitations persist:

1. Most simulations use a fixed turbulence model (commonly SST k- ω), without comparing alternatives like RNG k- ε or Realizable k-ε, despite their different sensitivities to shear, swirl and recirculation zones.
2. Pressure based boundary variation (to mimic physiological vascular resistance) is rarely used in parametric studies. Many instead control flow rate or RPM while maintaining fixed boundary conditions, which restricts analysis of head-flow behavior.
3. Non-Newtonian rheology is often excluded despite its known impact on near wall stress, platelet activation, and shear induced hemolysis, particularly at low shear regions or in transient simulations [14][20].

This thesis distinguish itself by addressing those gaps, Specifically, the simulation framework:

1. Compares results across multiple turbulence models to evaluate predictive accuracy and stability.
2. Uses pressure variation at the outlet (keeping inlet fixed) to construct full pressure flow performance curves.
3. Discusses non-Newtonian blood behavior in theory, while applying a Newtonian assumption justified by high shear rate operation in HeartMate 3 (Figure 7).

3.3 Problem Statement

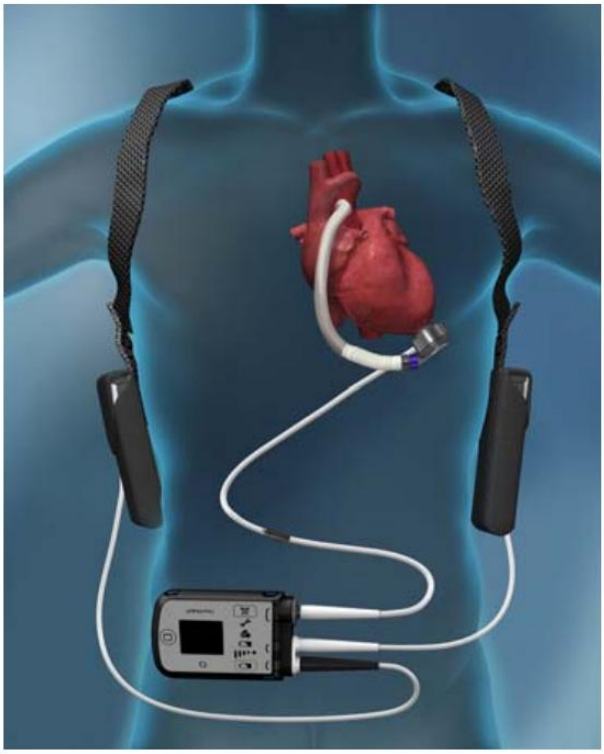

Figure 8. Position of a HeartMate 3 VAD in the abdomen. [17]

Despite these technological leaps, however, challenges remain. VADs have seen improvement in terms of manufacturing and creating efficient pumps available for a larger population, but they can be improved upon in terms of their design and efficiency. Current VADs require the user to carry an external bulky battery with them to support the rotary pumps functionality (Figure 8). Patients still face complications including gastrointestinal bleeding, pump thrombosis, infection, and stroke. A significant contributing factor to these issues is the complex internal fluid dynamics within VADs, which can generate regions of high shear, turbulence, and flow recirculation. These regions are closely linked to hemolysis (blood cell damage), platelet activation, and thrombus formation [24]. The pulsatile nature of the blood flow to be replicated by the rotary pumps is a field that needs to be studied and can be improved upon. [10] Consequently, a better understanding of the hemodynamic behavior of blood within rotary pumps is essential for optimizing performance, reducing complications, and extending the operational lifespan of these devices.

Although VADs pump designs have improved, if they can be improved to a better design, where the sizes might get smaller, with a similar or improved efficiency, while keeping the flow rate and pressure to replicate the blood flow within a heart with reduced chances

of damage to the heart, it would help a lot of people with heart diseases and might even help people not relying on a heart transplant procedure at all.

3.4 Research Objectives

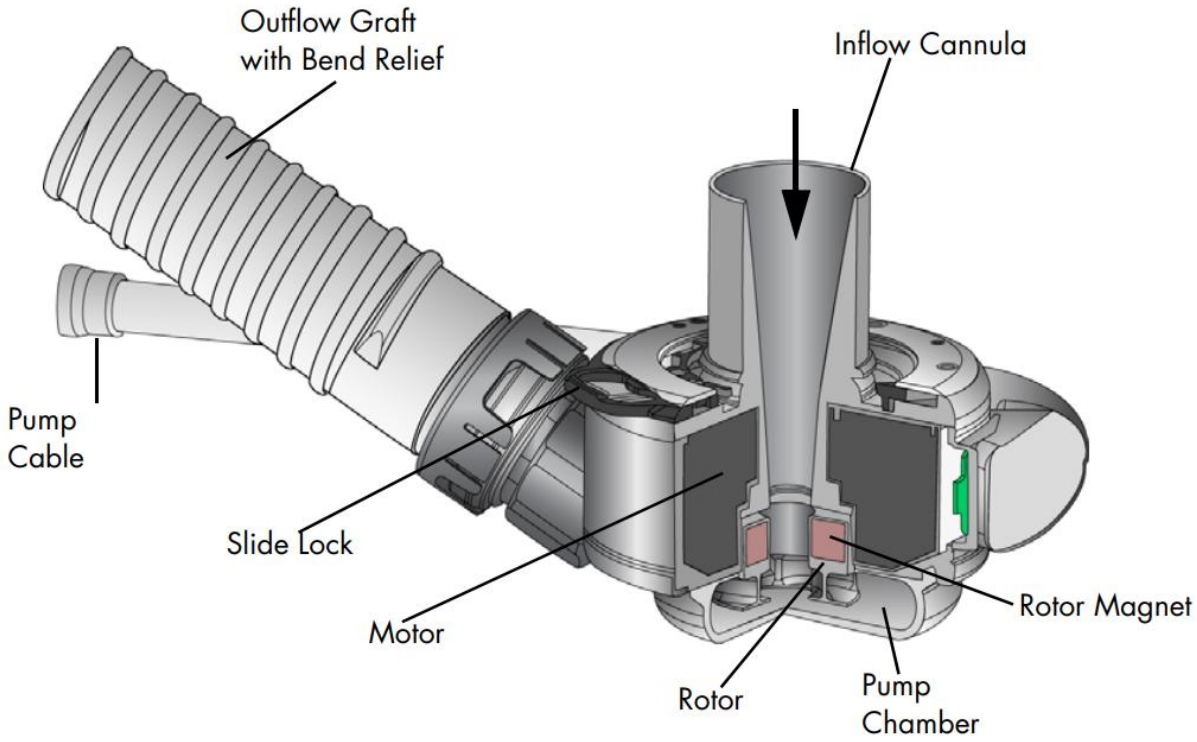

Figure 9. HeartMate 3 LVAD internal Components [21]

The HeartMate 3, developed by Abbott, is currently one of the most clinically successful and widely adopted LVADs. It utilizes a centrifugal design with a fully magnetically levitated rotor, permitting wide blood flow gaps and reducing shear-induced hemolysis. Additionally, it features a textured blood-contacting surface to promote endothelization and an intrinsic pulse mode to counteract the effect of continuous flow on the vasculature (Figure 9,52). Clinical trials such as the MOMENTUM 3 have demonstrated its superiority over older devices in terms of freedom from reoperation, pump thrombosis, and stroke [26].

However, as the internal geometry and the operational algorithms of HeartMate 3 are proprietary, independent academic research must rely on approximate models that capture the essential design and hydrodynamics(Figure 5,6,9,13,52). In this thesis, we will attempt to create a close geometry resembling HeartMate 3 and analyze the efficiency of HeartMate 3 with the documentation presented by Abbot analyzing the closeness in its pump curve (Figure 49) [21].

This is where Computational Fluid Dynamics (CFD) plays a transformative role. CFD enables the non-invasive visualization and quantification of flow fields, pressure distributions, wall shear stress, and the regions of potential blood damage within intricate geometries like those found in VADs. Through virtual prototyping, CFD significantly reduces the cost, time, and ethical challenges associated with experimental and clinical testing. More importantly, it allows for detailed, iterative design refinements before physical fabrication [25]. In the context of rotary blood pumps, CFD has been used to validate designs, optimize impeller blade angles, identify stagnation zones, and quantify shear rates, all of which are crucial to safe and efficient operation.

This thesis addresses this gap by creating a simplified, hydraulically representative CFD model inspired by the HeartMate 3, using ANSYS SpaceClaim for geometry creation and ANSYS Fluent for simulation. The study aims to evaluate pump performance under realistic boundary conditions and varying operational parameters. Using the Multiple Reference Fram (MRF) method, which allows steady state simulation of rotational effects, the model simulates blood flow through a rotating impeller and stationary stator region. Multiple turbulence models, including SST k-ω and RNG k-ε are compared to assess flow prediction accuracy. The influence of outlet pressure on flow rate is evaluated at constant RPMs to generate pump performance curves that include pressure vs flow rate, hydraulic power and efficiency metrics.

Furthermore, the Best Efficiency Point (BEP) – the operating condition where the pump achieves maximum hydraulic efficiency, is identified through post-processing of simulation data. The data is compared to documented FDA specifications of the HeartMate 3 and is used to evaluate the fidelity of the modeled design.

The results of this study aim to not only validate the proposed simplified model but also to demonstrate the utility of CFD in enhancing rotary blood pump performance and safety. The final model may serve as a foundation for future design optimization, flow-induced hemolysis studies, or even educational simulations for biomedical engineers and clinicians.

4 Theoretical Foundation

4.1 Working of a heart

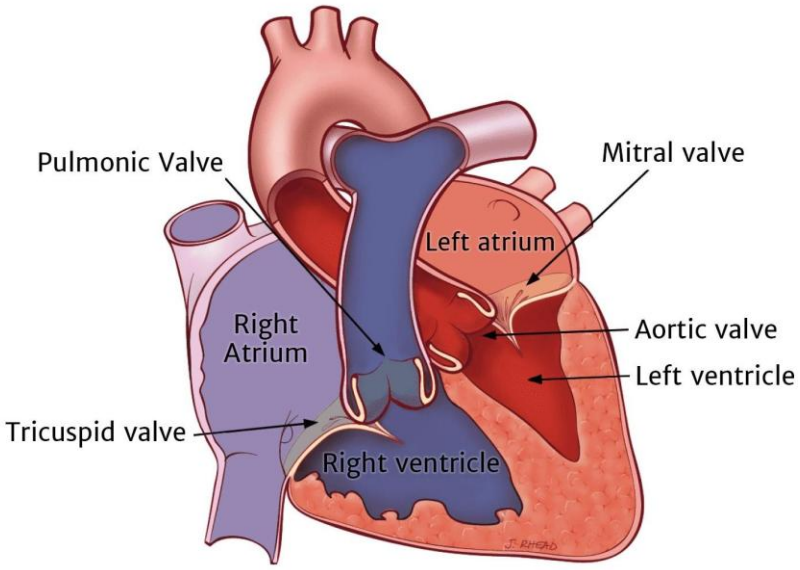

Figure 10. Simplified Anatomy of a Heart [51]

The human heart is a vital muscular organ responsible for circulating blood throughout the body. It functions as a dual pump, maintaining a continuous flow of oxygenated and deoxygenated blood in a closed-loop system. Structurally, the heart is composed of four chambers: the right atrium and right ventricle, which manage deoxygenated blood returning from the systemic circulation, and the left atrium and left ventricle, which handle oxygenated blood from the lungs. These chambers are regulated by one-way valves (tricuspid, pulmonary, mitral, and aortic valves) that maintain unidirectional flow during each cardiac cycle (Figure 10).

During a normal heartbeat, deoxygenated blood enters the right atrium via the superior and inferior vena cava. It then flows into the right ventricle, from where it is pumped through the pulmonary artery into the lungs for gas exchange. Oxygenated blood returns via the pulmonary veins into the left atrium, flows into the left ventricle, and is then ejected through the aorta into systemic circulation. The left ventricle plays a particularly crucial role in this process, generating the pressure needed to distribute blood to the entire body [34][35].

In patients suffering from heart failure, particularly left ventricular failure, the heart becomes unable to pump an adequate amount of blood to meet the metabolic demands of the body. This condition can stem from ischemic heart disease, dilated cardiomyopathy, or valve disorders, among other causes. Left-sided heart failure leads to a backlog of

blood into the pulmonary circulation, causing symptoms like fatigue, dyspnea, and fluid retention [2][11]. Over time, the weakened myocardium of the left ventricle fails to generate the required contractile force, reducing cardiac output significantly.

4.2 Fluid Dynamics and the Rotary Pump working principle

Fluid dynamics is the study of how fluids (liquids and gases) behave and interact under the influence of forces. In the context of rotary blood pumps such as HeartMate 3, fluid dynamics play a pivotal role in understanding and optimizing how blood is propelled through the circulatory system. This field encompasses the behavior of fluid particles, pressure variations, velocity distributions, shear stress, turbulence and energy transfer, all of which are fundamental to pump design and performance analysis.

Rotary blood pumps, especially those used in ventricular assistance devices (VADs), rely on the controlled manipulation of fluid mechanics to ensure continuous, non-pulsatile flow that meets the physiological demands of a patient with heart failure. Blood, as the working fluid in these systems, presents unique challenges because it is a complex, multiphase suspension that exhibits both Newtonian and non-Newtonian behavior depending on shear rates. In high-speed pumps like the HeartMate 3, the flow is typically treated as Newtonian due to the predominance of high shear regions where viscosity stabilizes [28].

The importance of understanding fluid dynamics lies in its direct impact on key aspects of pump performance, including efficiency, pressure generation, recirculation, shear stress and ultimately biocompatibility. Improper flow patterns within the pump can result in zones of stagnation or excessive shear, leading to hemolysis 9rutprue of blood cells), platelet activation or thrombus formation, all of which are critical risks in VAD therapy [3][30].

In rotary pumps, blood enters axially through the center of the rotor and is propelled radially outward by the rotating impeller blades. This transformation of axial to radial motion is governed by the centrifugal force imparted by the impeller. The impeller increases the kinetic energy of the fluid, which is then partially converted into pressure energy as the fluid exits the volume or diffuser region. The efficiency of this process depends on how well the fluid dynamics are managed withing the internal geometry of the pump [8].

Several complex phenomena define fluid behavior in rotary pumps:

- Flow Separation: Occurs when the fluid cannot adhere to the surface of the impeller or volute walls, causing detachment and recirculation.
- Secondary Flows: include vortices formed due to geometry-induced constraints like curvature and blade passage design,

- Turbulence: At high Reynolds numbers typical of VADs, turbulent flow is inevitable. It introduces chaotic fluid motion but also enhances mixing and energy dissipation.
- Wall Shear Stress (WSS): High WSS values, particularly near the blades or housing, are crucial indicators for hemolysis and must be carefully monitored using CFD simulations.

To simulate and analyze these phenomena, computational fluid dynamics (CFD) provides a virtual prototyping platform that soles the fundamental conservation equations of mass, momentum and energy (typically in a simplified, steady state for pump curve generation). The ability to visualize flow patterns, calculate performance parameters (e.g., head, torque, efficiency) and simulate design modifications makes CFD an indispensable tool for the development of blood pumps [26][27].

In this study, CFD was applied to simulate the internal flow within a simplified but hydraulically representative model of the HeartMate 3. The objective was to analyze how geometric configuration, operating speeds (RPM), and boundary pressures influence flow behavior, pressure rise and efficiency. The simulations included both steady-state and rotating reference frame techniques to replicate the rotor's motion and to evaluate the performance under various outlet pressure settings.

Moreover, capturing these fluid behaviors accurately depends on the mesh quality, boundary conditions, and turbulence models used. For instance, near-wall resolution through inflation layers was critical for model's boundary layer phenomena. Similar, the turbulence model selected had to resolve recirculation and adverse pressure gradients within the pump [3].

Understanding and mastering fluid dynamics in this context is not only about performance but also about patient safety. A VAD must be designed not just for optimal hydraulic behavior but also for minimizing shear-induced blood trauma. As such every design iteration and simulation strategy is built around principles rooted in fluid dynamics, making it a cornerstone of rotary pump engineering.

4.3 Navier Stokes equation

The Navier-Stokes equations form the foundation of fluid dynamics modeling and are central to the computational analysis of fluid flow in rotary blood pumps like the HeartMate 3. These equations represent the mathematical formulation of Newton's Second Law applied to fluid motion and describe how momentum is conserved in a moving fluid. They are coupled with the continuity equation, which enforces the conversation of mass. Together, they enable precise simulation of complex flow fields within biomedical devices where blood behavior must be predicted with high accuracy.

In CFD simulations of blood pumps, the Navier-Stokes equations are generally used in their incompressible, Newtonian form due to the assumption that blood density remains constant under physiological operating conditions. The two primary equations solved in this context are:

The Continuity equation (Mass Conservation:

$\nabla \cdot \mathbf{u} = 0$ (This means the net flow into a control volume equals the net flow out)

Where:

- ∇ is the **divergence of the velocity vector field**,
- u is the **fluid velocity vector** in m/s].

This equation states that the divergence of the velocity field is zero for incompressible flow, ensuring that the volume of fluid remains constant throughout the domain.

Momentum conservation (Navier-Stokes equation):

$$\boldsymbol{\rho}\left(\frac{\partial \bar{\boldsymbol{u}}}{\partial t} + \bar{\boldsymbol{u}} \cdot \boldsymbol{\nabla}\bar{\boldsymbol{u}}\right) = -\boldsymbol{\nabla} p + \boldsymbol{\mu}\boldsymbol{\nabla}^2\bar{\boldsymbol{u}} - \boldsymbol{\nabla} \cdot (\boldsymbol{\rho}\overline{\boldsymbol{v}'\boldsymbol{v}'}) + \bar{\boldsymbol{f}}$$

Where,

- $\boldsymbol{\rho}$ = fluid density [kg/m³]
- $\boldsymbol{u}$ = velocity vector [m/s]
- $\frac{\partial \vec{u}}{\partial t}$ = local (unsteady) acceleration
- $\vec{u} \cdot \nabla \vec{u}$ = convective acceleration (nonlinear term)
- ∇p = pressure gradient force [Pa/m]
- μ = dynamic viscosity [Pa·s]
- $\nabla^2 \vec{u}$ = viscous diffusion (Laplacian of velocity)
- v'= fluctuating quantities
- $\rho\overline{v'v'}$= Reynolds stress tensor
- $\bar{f}$ = Centrifugal or Coriolis forces

This formulation is appropriate for modelling blood inside VADs, where compressibility effects are negligible and flow velocities are moderate. The left-hand side of the Navier-Stokes equation accounts for the fluid's inertia while the right-hand side represents pressure and viscous forces acting on the fluid.

In the HeartMate 3 inspired CFD simulations, the Navier-Stokes equations were solved using ANSYS Fluent under steady-state conditions. The blood was modeled as a Newtonian fluid with density 1025 kg/m^3, viscosity 0.0035 consistent with the literature for high-shear blood flow conditions [14][28]. Steady-state modeling is sufficient when

investigating the performance curves of the pump (for e.g., pressure vs flow rate) rather than transient or pulsatile effects.

Due to the rotational nature of the flow, especially within the rotor region, a rotating reference frame (Multiple Reference Frame -MRF) was employed. The Navier-Stoles equations are modified in this rotating frame to include additional source terms accounting for Coriolis and centrifugal forces. These modifications are critical for accurately capturing the effects of impeller motion on the blood flow [3].

The equations are discretized using the Finite Volume Method (FVM), which integrates the governing equations over discreate control volumes. ANSYS Fluent applies schemes such as Second Order upwind for spatial discretization and SIMPLE (Semi-Implicit Method for Pressure Linked Equations) for pressure-velocity coupling to ensure numerical stability and accuracy [27].

While the equations themselves are well established, solving them accurately in the context of rotary blood pumps presents unique challenges:

- Complex Geometry: The impeller and volute shapes require finding meshes to resolve sharp gradients and narrow passages.
- High Reynolds number: Flow within the pump is typically turbulent, necessitating the use of turbulence models (discussed in upcoming sections).
- Boundary Layer Resolution: Capturing near-wall effect requires inflation layers and appropriate wall models (discussed in upcoming sections).
- Non-Newtonian Behavior: Although a Newtonian approximation is often sufficient for performance curves, the full equations can be extended to incorporate variable viscosity for more advanced hemocompatibility studies [14].

The strength of the Navier-Stokes framework is universality; once solved, the velocity and pressure fields obtained form the basis for computing all key performance metrics, including pump head, torque, hydraulic power and efficiency. They also allow the visualization of internal flow structures, such as recirculation zones and high shear regions, which directly inform pump optimization and patient safety considerations.

By systematically solving the Navier-Stokes equations across different operating conditions, varying outlet pressure, RPM or turbulence model, engineers can derive complete pump curves (H-Q, efficiency vs Q, power vs Q). These curves allow designers to pinpoint the Best Efficiency Point (BEP), identify flow-induces risks like cavitations or flow reversal and iteratively improve impeller designs.

Without this mathematical foundation, CFD simulations would lack predictive accuracy. Thus, the Navier-Stokes equations are not just a theoretical necessity but a practical tool

for translating the physics of blood flow into actionable engineering directions in VAD development.

4.4 Reynolds number

The Reynolds number (Re) is a fundamental, dimensionless quantity in fluid mechanics that characterizes the nature of fluid flow within a system. It provides a measure of the relative significance of inertial forces to viscous forces and is crucial for determining whether a flow is laminar, transitional, or turbulent. In the context of ventricular assist devices (VADs) like the HeartMate 3, the Reynolds number plays a central role in selecting appropriate turbulence models, predicting flow behavior, and assessing hemodynamic performance under physiological conditions.

The Reynolds number expresses the ratio of inertial forces (which cause the fluid to continue moving in its current direction) to viscous forces (which resist the motion and promote smooth, laminar flow). Low Reynolds numbers (typically < 2000) indicate laminar flow dominated by viscosity, while high Reynolds numbers (typically > 4000) indicate turbulent flow dominated by inertia and characterized by chaotic and unpredictable fluid motion.

In cardiovascular flows, Reynolds number varies significantly depending on the anatomical location and physiological condition. For example, in the aorta during peak systole, Re may exceed 6000, while in micro vessels it may be below 1. In the case of rotary blood pumps like HeartMate 3, the geometry and high rotational speed of the impeller generate flow conditions that result in Reynolds numbers ranging from 5,000 to over 50,000, depending on the region being evaluated [28][30].

The Reynolds number helps us define the model for the turbulence flow while using the Reynolds-Averaged Navier-Stokes (RANS). Time-averages the flow equations and models the entire turbulence spectrum using turbulence models like k-ε, k-ω, etc. This approach is computationally efficient and widely used in biomedical CFD. Due to the complexity of rotary blood pump geometries and the need for multiple parametric studies (e.g., varying RPM and outlet pressure), this study uses the RANS approach, specifically the SST k-ω and RNG k-ε models, to balance accuracy with feasibility [3][28][34].

4.5 Shear Stress Transport (SST) k-ω turbulence model

The Shear Stress Transport (SST) k-ω turbulence model is among the most advanced and widely adopted turbulence models for analyzing internal, rotating and high-shear fluid flows. Developed by Menter in the 1990s, the SST k-ω model combines the advantages of the standard k-ω model near walls and the k-ε model in the free-stream region, making it particularly well-suited for applications involving complex geometries, boundary layer separation and adverse pressure gradient conditions commonly encountered in ventricular assist devices (VADs) like the HeartMate 3.

The SST k-ω model belongs to the family of two-equation Reynolds-Averaged Navier-Stokes (RANS) models, which solve transport equations for:

- Turbulent kinetic energy (k): representing the intensity of turbulence.
- Specific dissipation rate (ω): describing the rate at which turbulent energy is converted into thermal energy through viscosity.

4.6 Renormalization Group (RNG) k-ε turbulence model

The Renormalization Group (RNG) k-ε turbulence model is a variant of the standard k-ω model, developed using a more rigorous mathematical approach based on renormalization group theory. This model introduces modifications to enhance accuracy in predicting turbulent flows with high strain rates, significant streamline curvature and rotation effects, which are common characteristics in rotating machinery and biomedical devices such as ventricular assist devices (VADs) like the HeartMate 3. In this study, the RNG k-ε model was employed as a secondary turbulence model for comparative analysis,

The RNG k-ε model solves two transport equations:

- Turbulent kinetic energy (k) – measures the energy contained in turbulent eddies.
- Turbulent dissipation rate (ε) – represents the rate at which this energy dissipates into heat due to viscosity.

These equations are similar in structure to the standard k-ε model, but they include additional terms that improve the model's ability to simulate the Swirling flows (caused by rotor blades in centrifugal pumps), the Strong streamline curvature (due to impeller geometry), the Rapid strain rates (in blade passages and narrow flow channels). These properties make the RNG k-ε model better suited than the standard k-ε model for blood pump simulations, where rotational and recirculating flows are prominent [3][29][36].

The active choice to chose this model apart from the SST k-ω model was because of previous studies done on the model for related studies. Boughner et al. [39] and Zhang et al. [40] can be seen as comparative studies that have shown the impact of turbulence model choice, which would include RNG k-ε.

4.7 Mass Flow rate

Mass flow rate is a foundational concept in fluid mechanics, and its precise determination is critical in the simulation, design, and performance evaluation of rotary blood pumps, including HeartMate 3. It not only determines the volume of blood delivered by the pump but also directly influences power output, efficiency, and clinical effectiveness. In the context of this thesis, mass flow rate is a core variable used to construct pump performance curves and evaluate the Best Efficiency Point (BEP) across different operating regimes.

The mass flow rate (m˙\dot{m}m˙) is defined as the mass of fluid passing through a given surface per unit time. It is mathematically expressed as:

Mass flow rate (Q) = ρ * A * v

where,

- Mass flow rate (Q) is in kg/s
- density (ρ) is in kg/m³(assumed 1025 kg/m³ for blood)
- area (A) is in m²
- velocity (v) is in m/s

In three-dimensional Computational Fluid Dynamics (CFD), Fluent computes mass flow rate by integrating the product of fluid density and velocity across the specified surface (inlet or outlet) of the fluid domain. The area-averaged or mass-averaged approach ensures precise numerical consistency [27].

4.8 Pressure Rise (ΔP)

Inlet pressure directly affects the net pressure difference that defines the pump's head and energy delivery:

ΔP = P outlet – P inlet

3.8.1 Head

Head represents the work done by the pump to increase the pressure energy of the fluid. It is defined as:

Total Pressure head (H) = (P outlet – P inlet) / (ρ * g)

Where:

- Total Pressure head (H) is in m.
- Area-weighted average static pressure at the outlet (P outlet) is in Pa
- Area-weighted average static pressure at the inlet (P inlet) is in Pa
- density (ρ) is in kg/m³(assumed 1025 kg/m³ for blood)
- Acceleration due to gravity (g) is in m/s²

This equation assumes incompressible flow, which is a valid approximation for blood in most cardiovascular applications due to its low compressibility and relatively stable density [28].

In practical terms, the head represents how high the pump could raise the fluid in a vertical column if it were discharged into the atmosphere. Although not used literally in VADs, this metric enables comparison across different pump designs and simulations.

4.9 Power

3.9.1 Hydraulic Power

Hydraulic power (Ph) is defined as the product of the mass flow rate of the fluid, the acceleration due to gravity, and the pressure head:

Hydraulic Power (Ph) = Q * g * H

Alternatively, when the pressure rise across the pump is known directly:

Hydraulic Power (Ph) = (Q * (P outlet – P inlet)) / ρ

Where,

- Hydraulic Power (Ph) is in W.
- Mass flow rate (Q) is in kg/s
- Total Pressure head (H) is in m.
- density (ρ) is in kg/m³(assumed 1025 kg/m³ for blood)
- Acceleration due to gravity (g) is in m/s² (assumed 9.81 m/s²)

This equation captures the useful work the pump performs on the fluid. It excludes energy lost to friction, turbulence, and internal recirculation and therefore represents the portion of mechanical energy that is effectively transferred to the blood.

Hydraulic power is especially important in VADs, where the goal is to augment or replace the native pumping function of the heart. In this context:

- A higher (Ph) implies that the pump is delivering sufficient energy to maintain systemic perfusion.
- A comparison of hydraulic and mechanical power allows efficiency calculation.
- Monitoring hydraulic power over time helps evaluate pump performance degradation or abnormalities.

Accurate prediction of (Ph) via CFD ensures that the designed pump meets clinical flow requirements (typically 4–6 L/min at physiological pressures) while maintaining acceptable energy demands [3][26].

3.9.2 Mechanical Power

Mechanical power (Pm) is mathematically expressed as the product of torque (τ) and angular velocity (ω):

Mechanical Power (Pm) = τ * ω

Where:

- Mechanical Power (Ph) is in W

- Torque applied to the rotor/impeller (τ) is in Newton-meters, N·m
- Angular velocity in radians per second (ω) is in rad/s

In rotary blood pumps, mechanical power is critical because:

1. It determines the electrical energy the motor must supply.
2. It influences the thermal load within the pump, potentially affecting surrounding tissues in implantable devices.
3. It enables the efficiency calculation by comparing it with hydraulic power (discussed in section 13).
4. It helps assess the mechanical robustness of the impeller design and bearing systems, especially in long-term support scenarios.

For HeartMate 3-like systems operating between 3000–9000 RPM, mechanical power ranges can vary from under 1 W at low flows to above 10 W at higher pressure differentials [32]. Managing and minimizing this requirement without sacrificing hydraulic output is a key engineering challenge.

4.10 Angular Velocity

Angular velocity (denoted as ω) is defined as the rate of rotation around a fixed axis and is expressed in radians per second (rad/s). It quantifies how fast the impeller of the pump is rotating and is directly proportional to the rotational speed given in revolutions per minute (RPM):

Angular velocity (ω) = 2 * π * RPM / 60

Where:

- Angular velocity (ω) is in rad/s
- Rotational speed is in RPM
- Mathematical constant pi (π) is assumed 3.1416

This conversion is necessary because most mechanical and fluid dynamics calculations—including those for torque and mechanical power—require angular velocity in SI units (radians per second), not RPM.

4.11 Efficiency

In fluid mechanics and turbomachinery, efficiency (η) is defined as the ratio of the useful energy output (hydraulic power) to the energy input (mechanical power):

Efficiency (%) = (Ph / Pm) * 100

Where:

- Hydraulic Power (Ph) is in W

- Mechanical Power (Ph) is in W

This expression yields a percentage that quantifies the effectiveness of energy transfer inside the pump. A value close to 100% indicates highly efficient energy conversion, while lower values suggest significant losses due to turbulence, friction, or recirculation.

4.12 Head Flow vs Mass Flow Rate

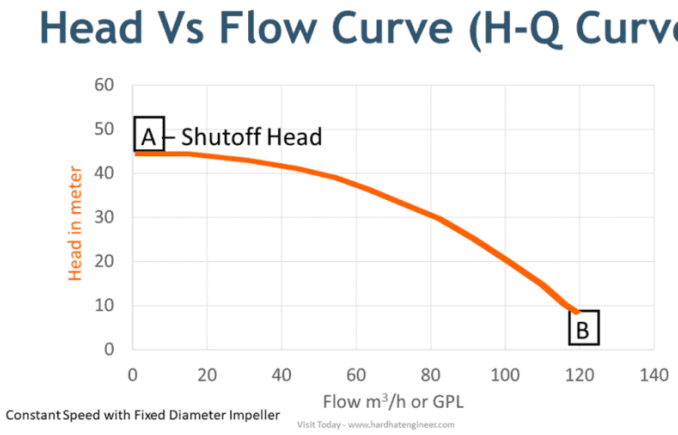

Figure 11. Exemplary plot of H-Q curve.

The Head–Flow (H–Q) Curve (Figure 11) is a fundamental performance characteristic used to evaluate and visualize the behavior of rotary pumps under different operating conditions. For rotary blood pumps such as the HeartMate 3, this curve provides insights into how the generated pressure (or head) changes in response to varying flow rates at a constant rotational speed. It is essential not only for performance validation but also for safe clinical operation, system design, and matching pump characteristics with patient-specific physiological needs.

The head–flow curve of a centrifugal pump like the HeartMate 3 generally exhibits a monotonically decreasing trend:

- At zero flow (shut-off condition), the head is at its maximum. This represents the maximum pressure the pump can develop when the outlet is completely blocked.
- As the flow rate increases, the head decreases because the impeller's energy is increasingly distributed into overcoming fluid inertia and resistance.
- At very high flow rates (approaching run-out condition), the head drops significantly due to reduced pressure generation capacity and potential flow separation or recirculation in the impeller.

This behavior is typical of centrifugal pumps and is distinct from positive-displacement pumps, which may maintain head across a range of flows.

4.13 Efficiency vs Mass flow rate

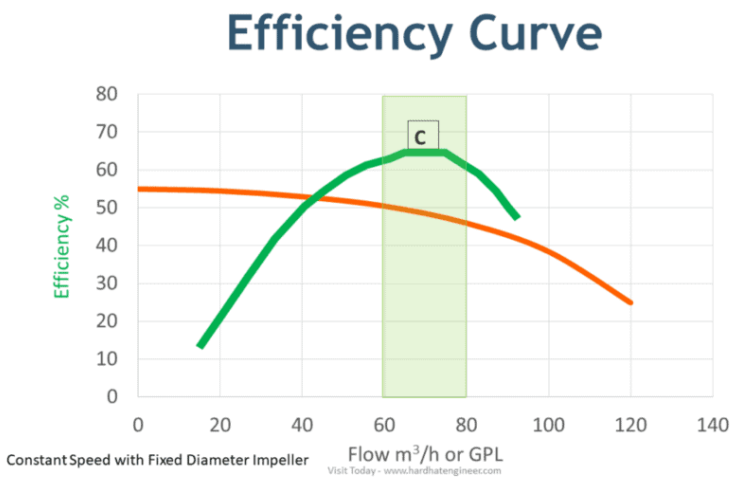

Figure 12. Exemplary plot of Efficiency-Q curve.

The Efficiency vs. Mass Flow Rate (η–Q) Curve (Figure12) is an essential performance indicator in the characterization of rotary pumps, particularly in biomedical applications such as Left Ventricular Assist Devices (LVADs) like the HeartMate 3. This curve illustrates how efficiently the pump converts mechanical energy (delivered via the motor to the impeller) into useful hydraulic energy imparted to the fluid across varying flow rates.

In contrast to the head–flow curve, which depicts pressure generation, the efficiency curve provides insight into energy utilization—a key factor in ensuring safe operation, reducing heat generation, minimizing power consumption, and extending device longevity in clinical settings.

The η–Q curve for a rotary pump typically exhibits a unimodal profile, rising from low efficiency at very low flow rates, reaching a maximum at the Best Efficiency Point (BEP), and then gradually declining as flow increases further:

- At very low flow rates (e.g., near shut off): Efficiency is poor due to leakage, recirculation, and dominance of frictional losses relative to useful energy output.
- Near the BEP: Optimal balance is achieved between flow rate, pressure generation, and internal energy losses. This is the most energy-efficient operating condition.
- At high flow rates: Efficiency declines due to flow separation, turbulence, and possible onset of backflow or cavitation, especially if the impeller design is not optimized for such conditions [26][27].

This curve provides crucial information for determining not only where the pump performs best but also where clinical or mechanical risks may arise if operated off-design.

5 Methodology

This section outlines the comprehensive computational workflow used to simulate, analyze and evaluate performance of a simplified HeartMate 3 rotary blood pump using Computational Fluid Dynamics (CFD). The overall objective was to investigate pressure-flow behavior and estimate pump performance using multiple turbulence models and boundary conditions across different operating speeds. This section outlines the design, meshing, simulation and performance evaluation methodology used to accomplish these objectives.

5.1 Geometry Creation

Figure 13. Heartmate 3 exploded view diagram [7]

The HeartMate 3 is a centrifugal rotary blood pump with a magnetically levitated rotor, engineered to minimize mechanical wear and enhance hemocompatibility. In the actual device, blood flows axially into the center of the rotor and is ejected radially outward by centrifugal force generated through impeller rotation (Figure 13). This architecture enables high efficiency and reduced hemolysis, which are essential considerations in both real-world use and computational simulations [16].

The initial geometry was constructed in ANSYS SpaceClaim using approximate dimensions and references available in open access figures (Figure 5,6,9,13,52) and publications [1][7][21]. The models include two primary components, the housing (stator) and the rotor (impeller). The rotor was placed concentrically inside the housing, and the region between the rotor and the housing was defined as the fluid domain.

The geometry was created in ANSYS SpaceClaim, designed to emulate the general structural and hydraulic design of the HeartMate 3 pump. Since the actual CAD geometry and internal specifications of the HeartMate 3are proprietary and not publicly accessible, a simplified but hydraulically representative model was developed. The model includes the following components:

1. Rotor assembly (impeller):

   Represented by a cylindrical rotor with curved blades. These blades were modeled based on standard centrifugal pump designs used in biomedical applications [3]. Positioned inside the housing, the rotor was modeled as a cylindrical core with attached blades. The blade design was based on typical biomedical impeller blade profiles, with careful consideration given to curvature, thickness and clearance [1].

2. Rotor housing (stator):
   The stationary part of the pump encases the rotor and defines the fluid domain boundaries, including inlet and outlet sections. This stationary part forms the outer boundary of the fluid domain and supports the overall structure of the pump. It features an axial inlet and a radial outlet, mirroring standard centrifugal flow paths.

After assembling the housing and rotor and aligning them appropriately, and confirming the geometry was watertight and free from defects, a volume extraction operation was performed to isolate the internal fluid zone. The area immediately surrounding the rotor was labeled as Actual_Rotatinng_Volume, while the remaining stationary fluid domain was labeled as Actual_Static_Volume. Figure 15(A) shows the design of the housing and the rotor, while Figure 14 highlights the volume extracted for simulation. The final dimensions of the housing and rotor are shown in Figure 15(A) and Figure(B).

The two fluid volumes extracted:

1. Rotating Fluid Volume (Actual_Rotating_Volume): Surrounding the rotor (defined as the rotating domain in Fluent).
2. Static Fluid Volume (Actual_Static_Volume): The rest of the pump casing.

This division allowed the simulation of rotational motion using the Multiple Reference Frame (MRF) method, where only the rotor-adjacent fluid region is rotated while the rest remains static.

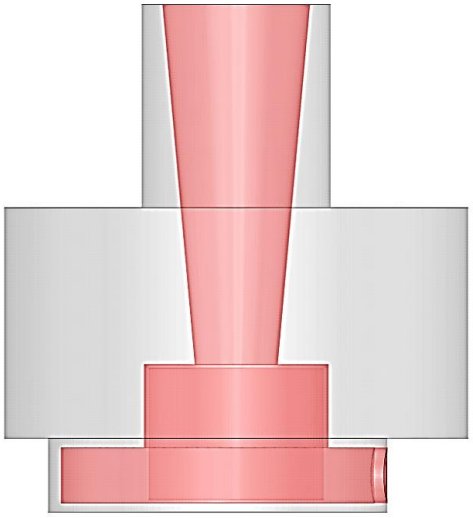

Figure 14. Volume extracted for the meshing show in red.

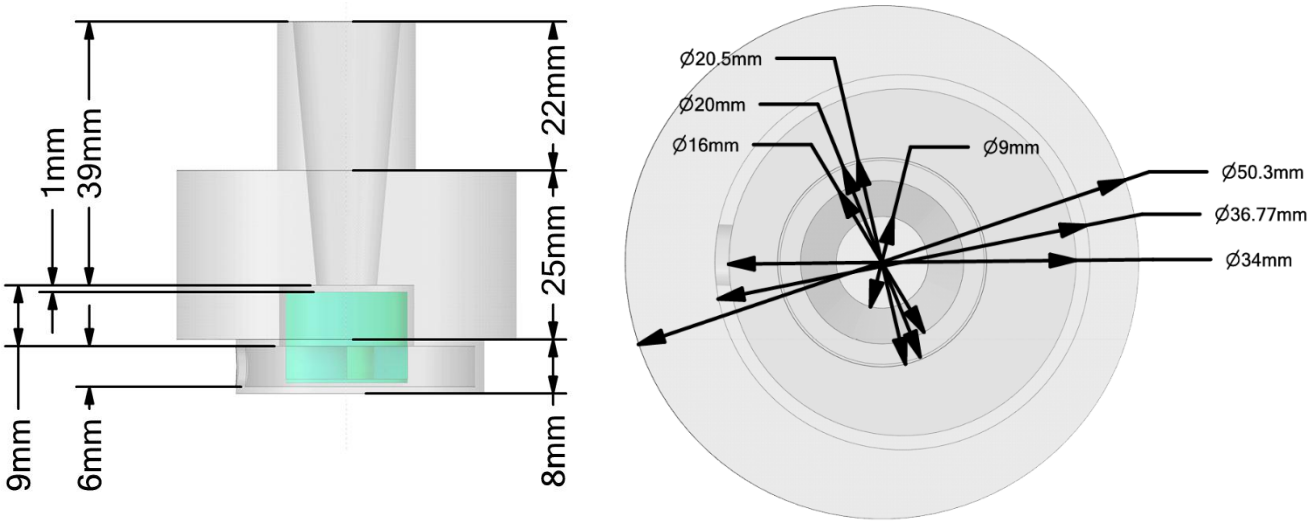

Figure 15(A). The schematic of geometry with rotor at the center.

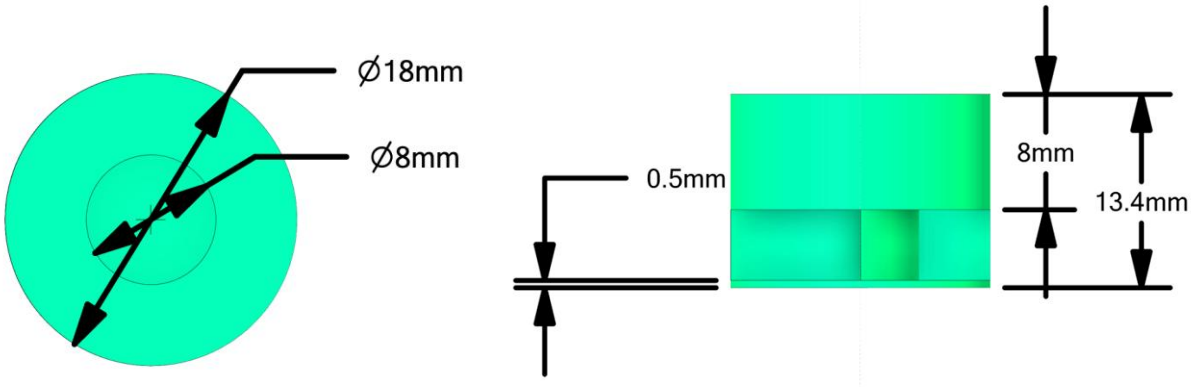

Figure 15(B). The schematic rotor.

The geometry was aligned along the Z-axis, with the rotor rotating about the same axis. Great care was taken to ensure proper contact between volumes and accurate placement of inlet and outlet surfaces to avoid mesh defects and overlapping interfaces.

These interfaces were designated as non-conformal to allow interpolation between disparate mesh sizes while preserving continuity and conservation laws.

For the model with the modified blades, the blades size was reduced by 20% from either open edge, and the sharp edges were rounded. The edges of the rotor wall were rounded (Figure 16 (c)).

Figure 16. Red regions showing the removed edges of the rotor of the base model and the new model with smaller and smoother edges.

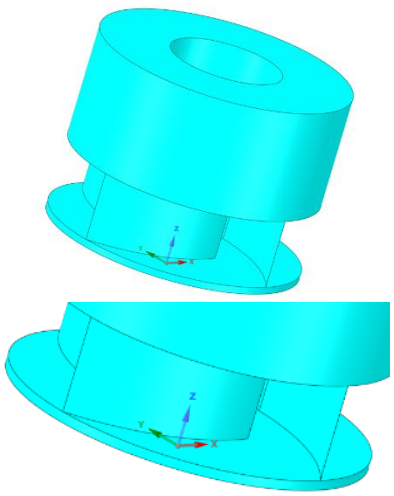

Figure 16 (a) Base Model Rotor.

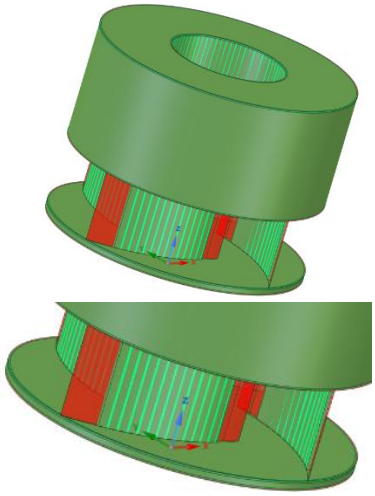

Figure 16 (b) Changes shown in red regions.

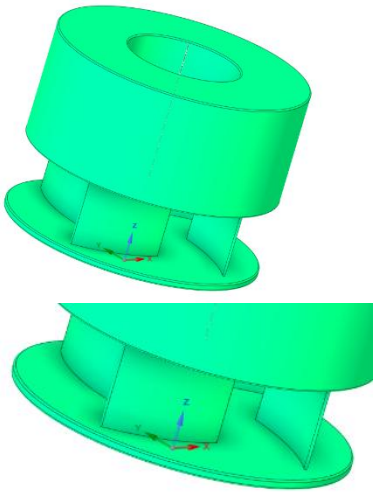

Figure 16 (c) Modified Rotor Blades

5.2 Mesh Generation

After geometry construction and volume extraction, the model was imported into ANSYS Meshing to perform volume discretization. Given the complexity of the rotary blood pump geometry, including the curved impeller blades and narrow fluid passages, generating a high-quality mesh was critical to ensure numerical accuracy and stability of the CFD simulation. The primary goal was to achieve a mesh under 1 million elements, satisfying both quality standards and the computational limits imposed by the ANSYS Fluent Student Version.

5.2.1 Base Model:

The meshing process for the base rotor model began by applying the following settings:

- Body sizing was set to 0.7 mm on both the rotor and the stator housing to ensure a uniform baseline refinement.

- Face sizing was applied to the rotor walls and blades, set to 0.3 mm, in order to prevent quality degradation in high-curvature areas.
- Inflation layers were applied:
    - On the stator housing (excluding inlet and outlet): 5 layers with a growth rate of 1.2.
    - On the rotor walls and blades: 5 layers, also with a growth rate of 1.2, to capture boundary layer effects and resolve near-wall shear stress accurately.

Although the mesh appeared visually consistent and acceptable for simulation purposes, the peak skewness value suggested that further refinement or adjustments were necessary, especially in critical areas near the rotor blades (Figure 17).

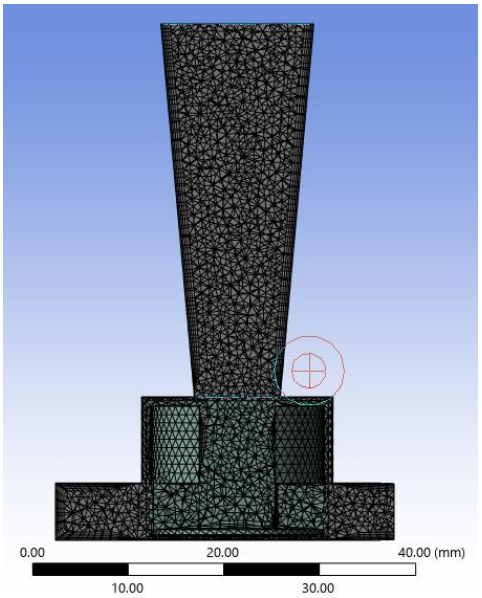

Figure 17 (a)

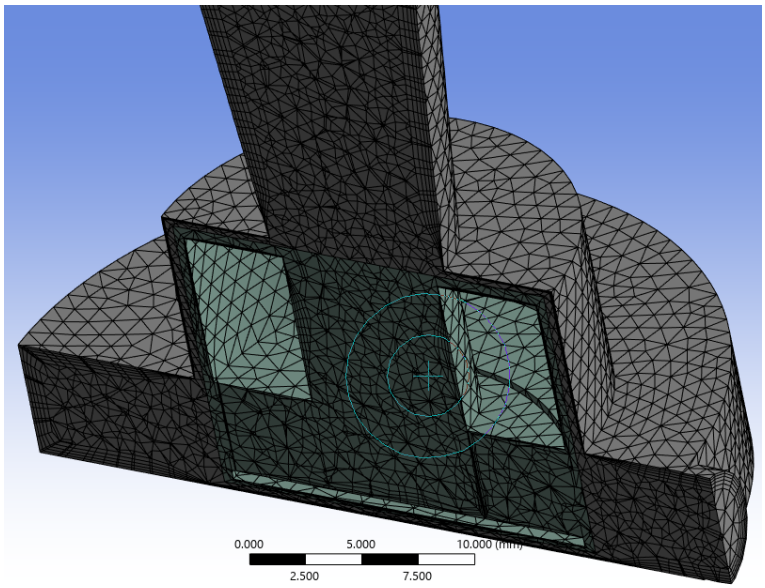

Figure 17 (b)

Figure 17 (a). Sectioned side view of mesh of the extracted volumes; Figure 12 (b) Zoomed in sectioned view of the mesh of the extracted volumes at an angle (Base Model)

5.2.2 Modified Blade Model

The modified rotor blade geometry, designed to improve blade aerodynamics and reduce hemolysis risk, introduced additional complexity in meshing due to new rounded blade edges (fillets). Applying the same meshing strategy from the base model resulted in a drastic increase in mesh count, exceeding 5 million elements, which made it un-processable within the student version of ANSYS Fluent (Figure 16 (c)).

The excessive refinement was localized primarily around the curved fillet regions at blade edges, where the meshing algorithm automatically generated extremely fine elements to resolve curvature accurately. This resulted in a prohibitively large element count, despite maintaining high-quality metrics.

To address this, a mesh optimization strategy was employed, focusing on curvature-based refinement control and manual local sizing overrides:

- Advanced Sizing Function was enabled with curvature control, and Local Minimum Size parameters were adjusted:
    - 0.1 mm for rotor blade surfaces
    - 0.2 mm for rotor walls
    - 0.8 mm for stator housing surfaces
- Updated sizing settings:
    - Rotor blade face sizing: increased to 0.5 mm
    - Rotor walls: set to 0.8 mm
    - Stator housing: set to 1 mm

These adjustments reduced the mesh density in overly refined regions without compromising resolution in high-gradient zones.

The final mesh for the modified rotor blade model resulted in 651,164 elements, successfully remaining under the student version's threshold. The final mesh quality metrics were:

- Maximum skewness: 0.9487
- Average skewness: 0.3000
- Maximum orthogonal quality: 0.9926
- Average orthogonal quality: 0.6900

These values are well within accepted meshing standards. Specifically, orthogonal quality values above 0.65 and skewness below 0.95 are considered suitable for high-accuracy CFD simulations of rotating turbomachinery flows [27].

The mesh was visually verified using cross-section views to ensure continuity across the rotating and static interfaces. Contact regions were cleaned, and all named selections were verified for consistency with boundary condition setup. The geometry was imported into ANSYS Meshing, where a structured volumetric mesh was generated. Maintaining mesh quality was vital to ensure accuracy and convergence (Figure 18).

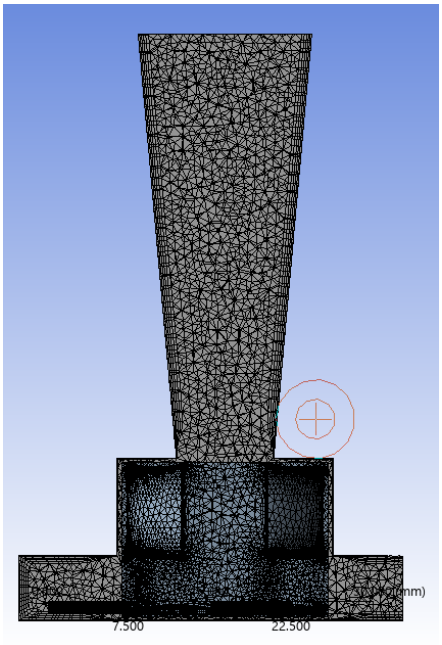

Figure 18 (a)

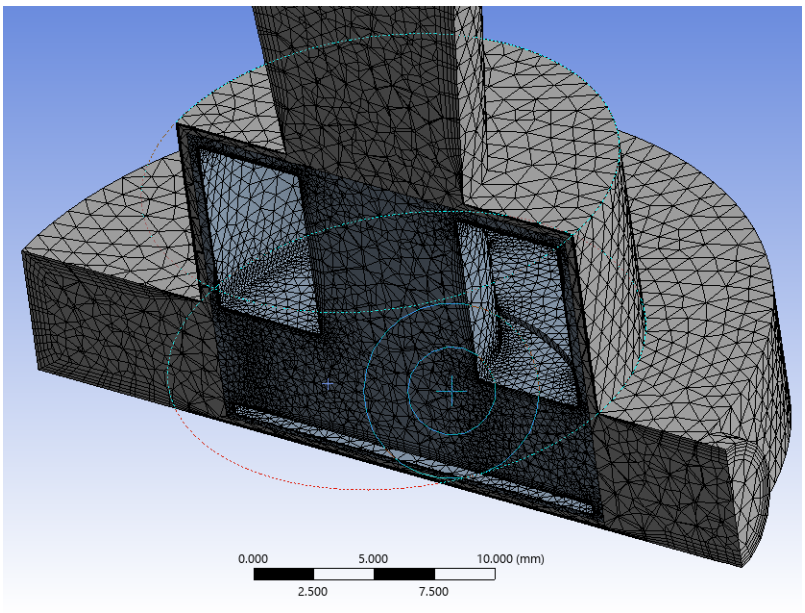

Figure 18 (b)

Figure 18 (a). Sectioned side view of mesh of the extracted volumes; Figure 13 (b) Zoomed in sectioned view of the mesh of the extracted volumes at an angle (Modified Blades Model)

5.3 Creating named selections

Accurate boundary condition assignment is essential in computational fluid dynamics (CFD) simulations, particularly for complex internal flow domains such as those in rotary blood pumps. To streamline this process and ensure clarity during solver setup in ANSYS Fluent, a comprehensive set of named selectins was created in ANSYS Meshing. These labels serve not only as a means of organizing different mesh regions but also enable precise specification of physical conditions such as wall motion, reference frames, and interfaces.

The following named selections were defined:

- Housing_Walls: This selection includes all internal wall surfaces of the pump's stationary housing (stator). These Walls interact with the flowing blood and influence boundary layer formations and the wall shear stress (WSS), which are important for hemocompatibility assessment in ventricular assist devices (VADs) [3][14].
- Rotor_Walls: This group comprises all surfaces of the rotor except the impeller blades. It includes the impeller hub, side walls and any internal rotor surfaces not involved in active fluid acceleration. These walls were assigned rotational motion using the Multiple Reference Frame (MRF) method to simulate the pump's impeller rotation.

- Rotor_Blades: This specific selection isolates the walls of the rotating impeller blades. These surfaces are the primary energy-transferring components in the pump, directly responsible for imparting kinetic energy to the blood and generating pressure rise. They are of particular interest in CFD post-processing, especially when evaluating torque, pressure leading and flow separation phenomena near blade surfaces [3][20].
- Interface_Rotor: This selection defines the boundary between the rotating fluid volume (Actual_Rotating_Volume) and the adjacent static region. It represents the side of the fluid-fluid interface that is part of the rotating reference frame. Setting this interface properly is critical for data exchange between the rotating and static zones during simulation. A non-conformal mesh interface was used, allowing interpolation between different mesh densities on either side, as supported by ANSYS Fluent's MRF implementation [22].
- Interface_Stator: The complement to Interface_Rotor, this selection includes the portion of the static volume (Actual_Static_Volume) that connects to the rotating region. Together, the Interface_rotor and the Interface_stator form a continuous data pathway across which flow variables such as velocity, pressure and turbulence quantities are transmitted.
- Inlet: The inlet surface was defined at the axial entry point of the pump. It was set as a Pressure inlet boundary condition in Fluent with a gauge pressure of 0 Pa to simulate blood entry from a low-pressure ventricle. This reflects common clinical configuration in left ventricular assist devices (LVADs), where the inflow cannula draws blood from the left atrium or ventricle [19].
- Outlet: The outlet surface corresponds to the radial exit port of the pump. It was defined as a Pressure Outlet and its value was varied across simulations to simulate different downstream vascular resistance. Varying the outlet pressure at constant rotor speed enables the construction of pump performance curves (Head vs. Flow Rate and Efficiency vs Flow Rate) [3][21].

These named selections also facilitated the post-processing of CFD results by enabling targeted extraction of key flow variables from the relevant geometry regions. This nomenclature not only improves simulation accuracy but also ensures reproducibility and clarity in performance metric calculations.

5.4 Simulation Setup in Fluent

All computational simulations in his study were conducted using ANSYS Fluent (2025 R1 Student Edition). The Fluent module was selected for its advanced capabilities in handling complex internal flow simulations, rotating reference frames and turbulence modeling which are essential for replicating for hemodynamics of rotary blood pups. A structured

and validated CFD workflow was followed for each simulation, ensuring repeatability, accuracy and convergence.

The following section describes the sequential steps taken in Fluent for setting up and solving each simulation case.

5.4.1 General Setup and Mesh Verification

After importing the mesh from ANSYS Meshing into Fluent, the General settings were reviewed to ensure correctness of mesh units and coordinate orientation. The geometry was verified to be aligned along the Z-axis, which is consistent with the rotation axis of the rotor in centrifugal pumps. A visual inspection was conducted to ensure the mesh had imported correctly, particularly at critical interface regions such as rotating-static volume interfaces and absence of negative cell volume or highly skewed elements.

5.4.2 Physical Models

The simulation used a pressure based, steady-state solver with absolute velocity formulation. The energy equation was disabled, assuming isothermal flow due to the negligible thermal gradients required for a hydraulic analysis for this pump.

Turbulence modeling enabled us to capture the inherently high Reynolds number, turbulent flow within the pump. Two turbulence models were used for comparative analysis:

- SST k-ω model: Selected for the base simulation due to its strong performance in resolving near wall behavior and boundary layer separation [3].
- RNG k-ε model: Used for comparative simulations, particularly suitable for swirling and rotating internal flows [3][20].

These models are both two equation Reynolds-Averaged Navier-Stokes (RANS) models capable of accurately resolving turbulent structures in turbomachinery applications.

5.4.3 Material Properties

The fluid was defined as blood, treated as a Newtonian fluid in the base simulations. The properties assigned were:

- Density: 1025 kg/m³
- Dynamic Viscosity: 0.0035 Pa·s

These values were taken from literature sources as representative for blood at high shear rats, where it behaves Newtonian [14][20].

5.4.4 Cell Zone Conditions and Reference Frames

The fluid domain was divided into two volumes:

a. Actual_Rotating_Volume (rotor-adjacent fluid region)
b. Actual_Static_Volume (rese of the pump casing)

To simulate rotor motion, the Multiple Reference Frame (MRF) method was used. This technique assigns rotational motion to the Actual_Rotating_Volume without requiring transient sliding meshes, making it suitable for stead-state simulations of rotating equipment [22].

- Rotational Speed: Simulations were conducted at 3000, 5000, 7000 and 9000 RPM, which is within the clinically recommended range for HeartMate 3 operation [21].
- Rotation Axis: The Z-axis was specified as the axis of rotation.

The static region was kept motionless and interacted with eh rotating region via mesh interfaces.

5.4.5 Boundary Conditions

Boundary conditions were assigned as follows, based on the named selections created earlier:

- Inlet: Defined as a Pressure Inlet with a gauge pressure of 0 Pa, simulating blood entry from a low-pressure atrial chamber. In this study, Pressure Inlet was defined as the CFD boundary condition at the entry to the pump. The boundary was set with a gauge pressure of 0 Pa, simulating atmospheric conditions and enabling internal flow to be determined by the outlet pressure and the pump's rotational energy input. This approach is standard in open-loop simulations, where the objective is to assess performance across a range of system loads rather than reproduce exact cardiovascular loop dynamics [1][3].
- Outlet: Defined as a Pressure Outlet, with values incrementally (from 0 Pa up to reverse flow threshold) to simulate different systemic resistances and create a full pump performance curve.
- Walls: All statis and rotating surfaces (Housing_Walls, Rotor_Walls, Rotor_Blades, Interface_Stator, Interface_Rotor) were assigned no-slip boundary condition. Rotating walls were specified in the rotating frame to correctly simulate mechanical interaction.
- Interfaces: the fluid-fluid interface between the rotating and static regions was created using a non-conformal mesh interface, pairing Interface_Stator and Interface_Rotor.

These settings allowed consistent modeling of internal flow behavior under different operational conditions.

5.4.6 Monitors and Initialization

Hybrid initialization was used to generate a starting solution that balances velocity, pressure and turbulence variable, reducing the number of iterations required for convergence. Monitoring was essential to ensure solution stability and convergence:

Report Plots Configured:

- Torque (Moment): On Rotor_Walls and Rotor_Blades about the Z-axis (Nm).
- Mass Flow Rate: At the inlet.
- Static Pressure: At both the inlet and outlet
- Scaled Residuals: Continuity, momentum and turbulence quantities.

These variables were plotted and monitored during every run to determine the point of convergence.

6 Results & Discussions

This section systematically presents and interprets the simulation results obtained from the Computational Fluid Dynamics (CFD) analysis of the Ventricular Assist Device (VAD) models. The focus is on quantifiable performance metrics such as head, mass flow rate, efficiency, and power, as well as qualitative observations of flow phenomena, analyzed across different rotational speeds, turbulence models, and a blade-modified design.

The results are categorized by:

- Turbulence model used: SST k-ω and RNG k-ε
- Pump configuration: Base Model and Blade Modified Model
- Operating RPMs: 3000, 5000, and 7000
- Key performance parameters: Head vs. Flow Rate, Efficiency vs. Flow Rate, and Power vs. Flow Rate

Each section evaluates simulation results, identifies the Best Efficiency Point (BEP), discusses shut-off conditions (zero flow), and compares performance with published data for the actual HeartMate 3 pump. Visualizations, charts, and computed metrics provide insight into the fluid dynamics and effectiveness of each configuration.

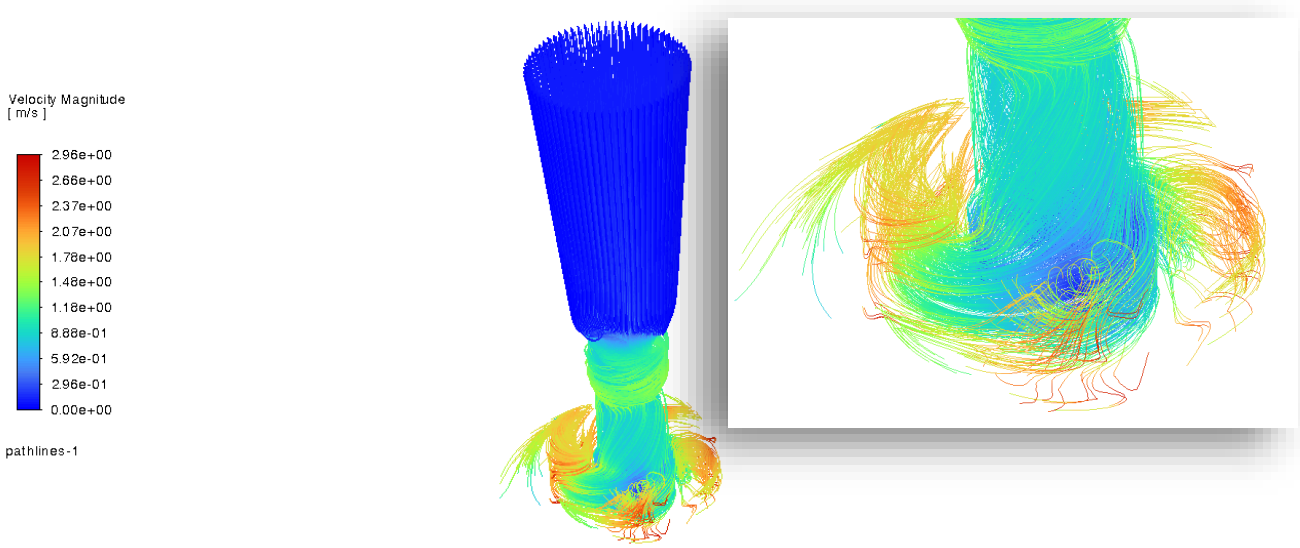

Figure 19. Pathline simulation of the flow through the Inlet.

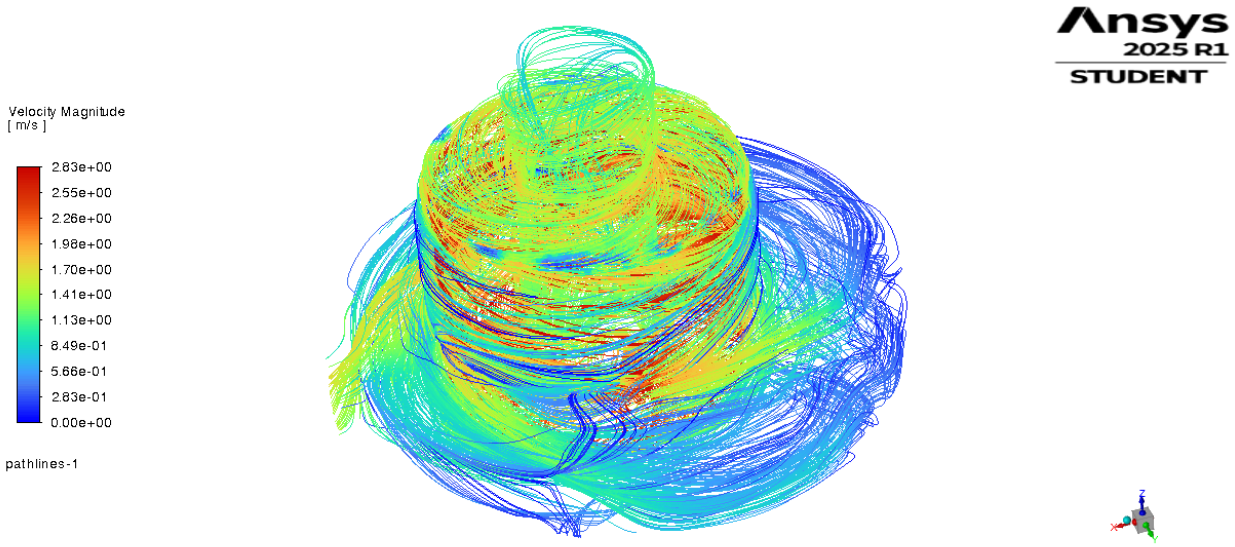

Figure 20. Pathline simulation of the flows through the Rotor.

The pathlines (Figure 19) and (Figure 20) offer a compelling qualitative representation of the fluid's complex journey through the pump, demonstrating the model's ability to effectively guide the flow. As observed, the fluid initially enters axially from the designated inlet. Upon reaching the rotating impeller, the rotor's action efficiently pulls the fluid inward towards its center. Subsequently, the centrifugal force generated by the rotating blades, through their carefully designed openings, effectively expels the fluid radially outwards. This outward moving fluid then interacts with the stationary pump housing walls, where its kinetic energy is partially converted into pressure, before it is finally discharged through the outlet.

Furthermore, these visualizations implicitly support the operational principle of magnetic levitation. While not directly modeled, the flow patterns confirm that a portion of the fluid dynamically surrounds the rotor. This hydrodynamic interaction is crucial in advanced VADs like HeartMate 3, where the fluid itself contributes to keeping the rotor suspended and rotating without mechanical contact, thereby minimizing friction, wear, and the need for traditional bearings.

6.1 Base Model Performance (SST k-ω)

The base model, simulated with blood treated as a Newtonian fluid and using the SST k-omega turbulence model, provided foundational performance characteristics.

6.1.1 3000 RPM Analysis

The pump curve for 3000 RPM showed the relationship between mass flow rate and head, indicating effective pressure generation at this speed. At 3000 RPM, the SST k-ω model demonstrated a typical centrifugal pump behavior. The Head vs. Flow Rate curve in Figure 21 shows a descending trend, where head decreases as flow increases, which is indicative of increasing system demand.

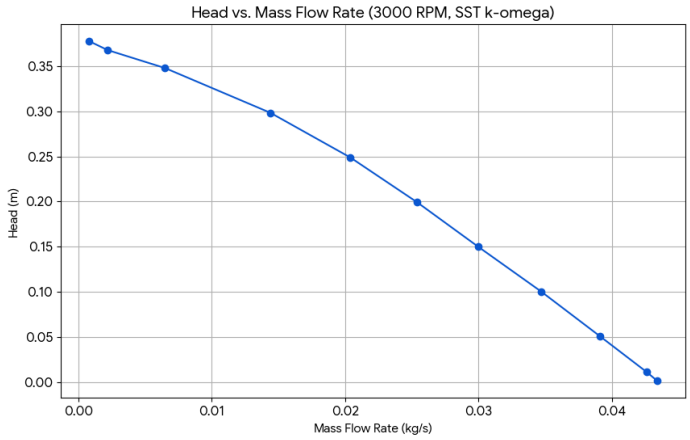

Figure 21. Pressure Head vs Mass Flow Rate of the Base model at 3000 RPM (SST k-ω)

The maximum head (shut-off) occurs near zero flow and is approximately 0.37 m, at an outlet pressure boundary condition (BC) of 3700–3800 Pa. At this point, mass flow rate becomes nearly zero or negative, marking the pump's limit to overcome backpressure (Figure 21).

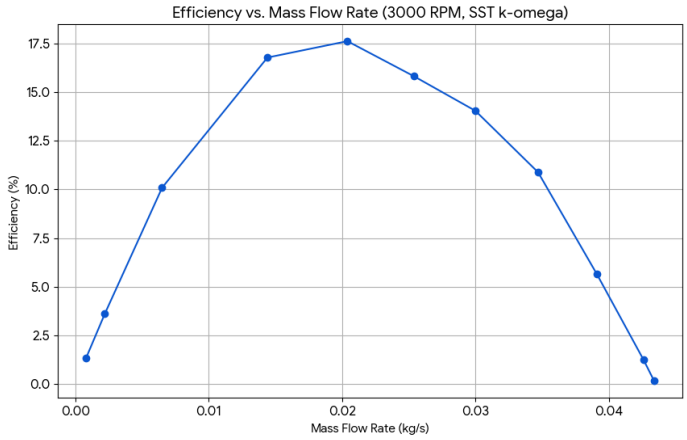

Figure 22. Efficiency vs Mass Flow Rate of the Base model at 3000 RPM (SST k-ω)

The efficiency curve peaked, defining the best efficiency point (BEP) for this operating condition. The Best Efficiency Point (BEP) occurs around a flow rate of 0.0204 kg/s (≈1.49 LPM), at 2500 Pa BC, where efficiency peaks at ~17.6%. This point reflects the most energy-efficient operating condition at this RPM (Figure 22).

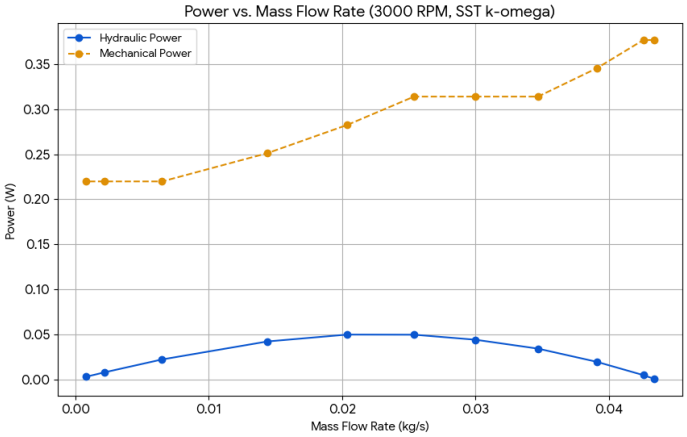

Figure 23. Power vs Mass Flow Rate of the Base model at 3000 RPM (SST k-ω)

Power curves illustrate hydraulic and mechanical power, demonstrating the energy conversion within the pump. Figure 23 indicates a nearly linear increase in mechanical power due to constant torque and rising angular velocity, while hydraulic power shows a nonlinear trend. This discrepancy is due to changes in both flow rate and pressure rise across the pump.

Overall, the 3000 RPM performance validates the expected centrifugal behavior: strong pressure at low flows, peak efficiency at mid-flows, and diminished performance at high flow conditions due to insufficient pressure buildup.

6.1.2 5000 RPM Analysis

At 5000 RPM, the pump exhibited higher head generation, and a different efficiency profile compared to 3000 RPM, reflecting the impact of increased rotational speed on performance.

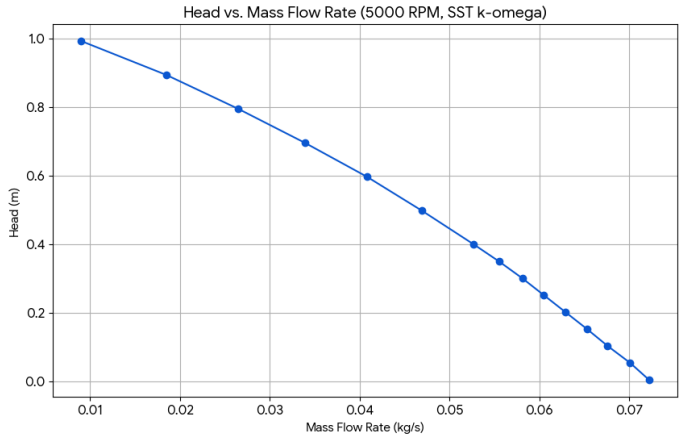

Figure 24. Pressure Head vs Mass Flow Rate of the Base model at 5000 RPM (SST k-ω)

The shut-off head occurs around 11000–12000 Pa BC, beyond which the flow starts to reverse. Maximum pressure head reaches approximately 1 m (Figure 24).

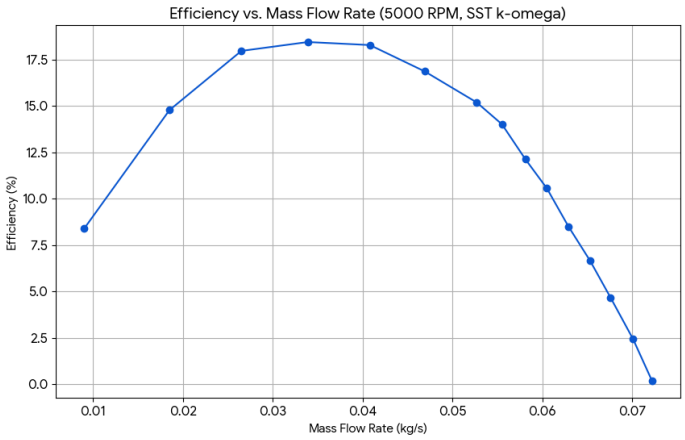

Figure 25. Efficiency vs Mass Flow Rate of the Base model at 5000 RPM (SST k-ω)

BEP is observed at 7000 Pa BC with a mass flow rate of ~0.0339 kg/s (≈1.98 LPM), and efficiency peaking at ~18.44%. Compared to 3000 RPM, the BEP shifts to higher flow and head values, demonstrating increased pump capacity. The efficiency curve (Figure 25) shows a broader peak compared to 3000 RPM, suggesting a wider optimal operating range.

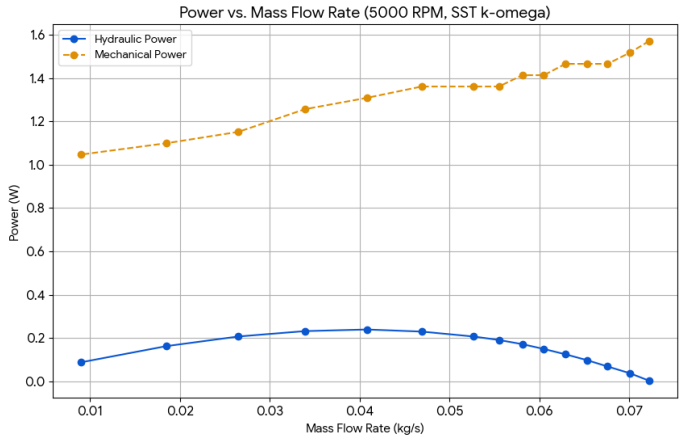

Figure 26. Power vs Mass Flow Rate of the Base model at 5000 RPM (SST k-ω)

In Figure 26, hydraulic power increases until BEP and then tapers off, while mechanical power continues rising due to increased torque demand.

6.1.3 7000 RPM Analysis

Further increasing the RPM to 7000 led to even higher head and different efficiency characteristics, indicating the pump's scalability with speed.

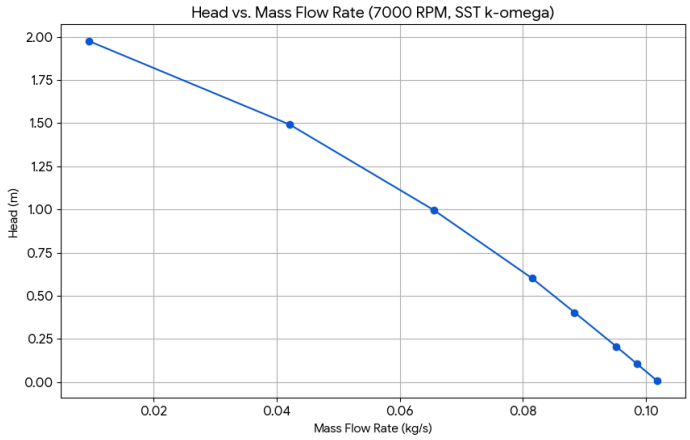

Figure 27. Pressure Head vs Mass Flow Rate of the Base model at 7000 RPM (SST k-ω)

Maximum head exceeds 1.97 m, at very low mass flow rates, indicating substantial pressure potential under occlusive conditions (Figure 27).

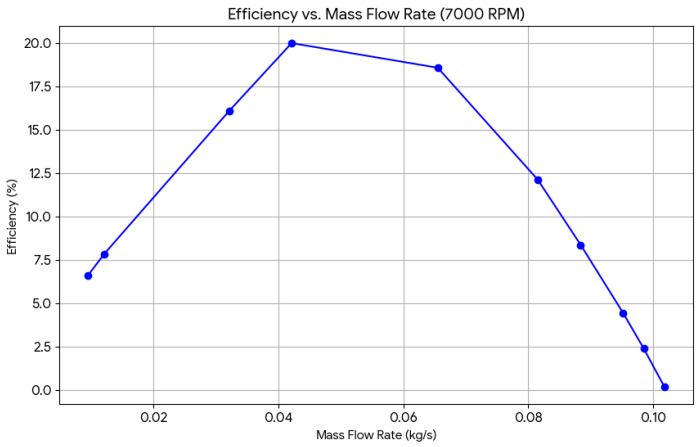

Figure 28. Efficiency vs Mass Flow Rate of the Base model at 7000 RPM (SST k-ω)

The BEP is observed at 15000 Pa BC, with a mass flow rate of ~0.0421 kg/s (~2.46 LPM) and peak efficiency of ~20.02% (Figure 28). This marks the highest efficiency across all tested RPMs.

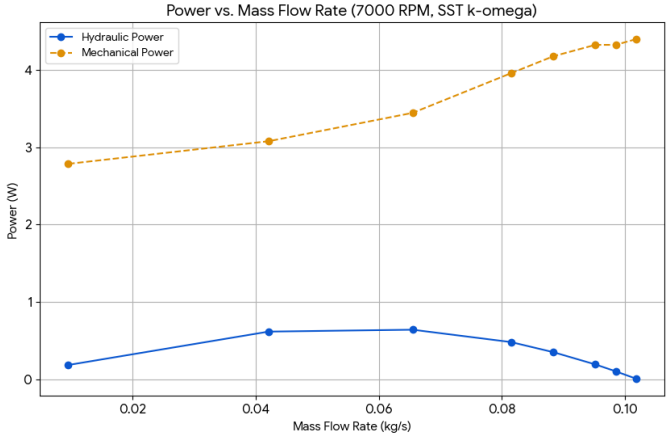

Figure 29. Power vs Mass Flow Rate of the Base model at 7000 RPM (SST k-ω)

Hydraulic power rises until BEP and then diminishes slightly, while mechanical power keeps rising due to increasing torque and speed (Figure 29).

6.1.4 Comparison of RPMs

Comparing the head vs. mass flow rate across 3000, 5000, and 7000 RPM revealed a clear trend: higher RPMs resulted in a greater head generated for a given flow rate.

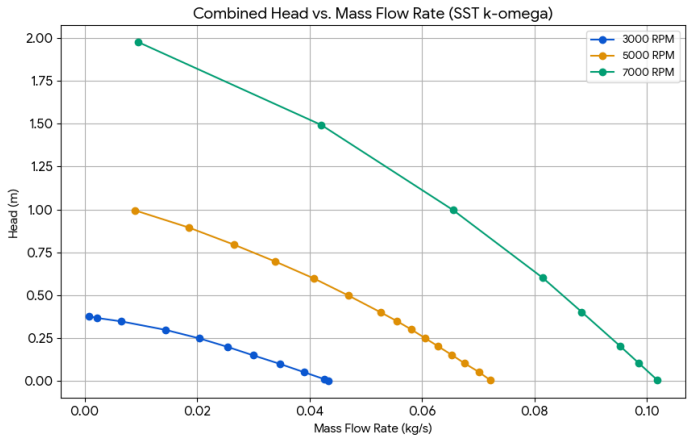

Figure 30. Pressure Head vs Mass Flow Rate of the Base model comparing 3000,5000 and 7000 RPM (SST k-ω)

In Figure 30, as RPM increases, the head-flow curve shifts upward and rightward, reflecting increased pressure generation and flow capacity. The shut-off head rises from ~0.37 m (3000 RPM) to over 1.97 m (7000 RPM), confirming greater backpressure resistance at higher speeds.

Similarly, higher RPMs generally shifted the efficiency curves, often leading to increased peak efficiency and a broader optimal operating range.

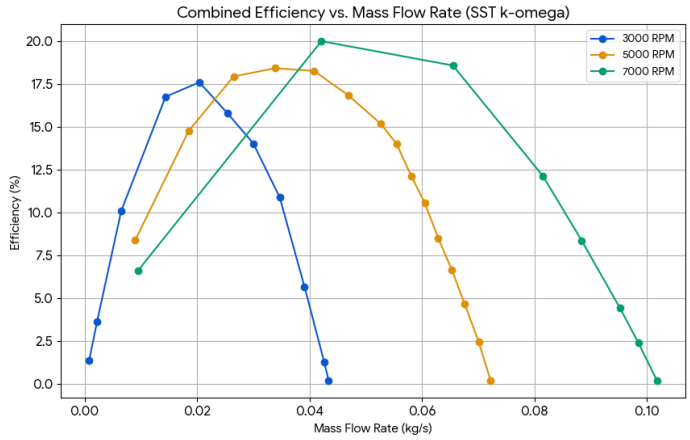

Figure 31. Efficiency vs Mass Flow Rate of the Base model comparing 3000, 5000 and 7000 RPM (SST k-ω)

In Figure 31, the efficiency curves broaden and shift with increasing RPM. While 3000 RPM shows peak efficiency at ~17.62%, 7000 RPM achieves up to ~20%. Additionally, BEP shifts toward higher flow rates and heads, as expected with increasing pump energy input.

These comparisons validate the simulation's ability to capture realistic pump dynamics across operational conditions, showing that SST k-ω produces consistent and physically plausible results across the full tested range.

6.2 Base Model Performance (RNG k-Ɛ)

Simulations were also performed using the RNG k-epsilon turbulence model at 3000 RPM. This model produced similar but distinct head, efficiency, and power curves.

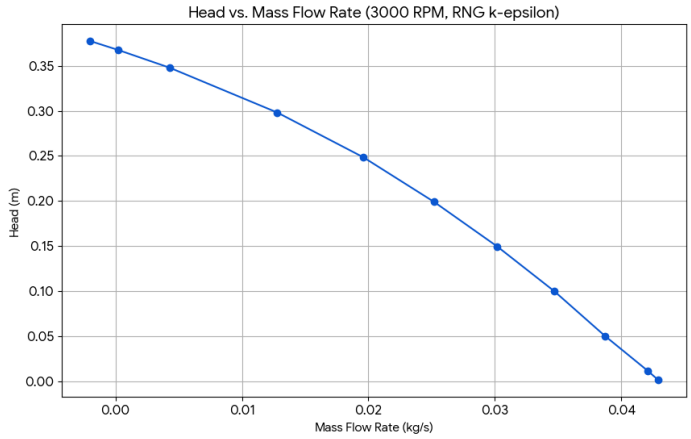

Figure 32. Pressure Head vs Mass Flow Rate of the Base model at 3000 RPM (RNG k-Ɛ)

The head-flow curve (Figure 32) follows a similar trend to SST k-ω, with head decreasing as flow increases. The shut-off head occurs at ~0.37 m (at 3800 Pa), consistent with the SST model, though slightly delayed due to differences in how turbulence is modeled near walls and recirculating zones.

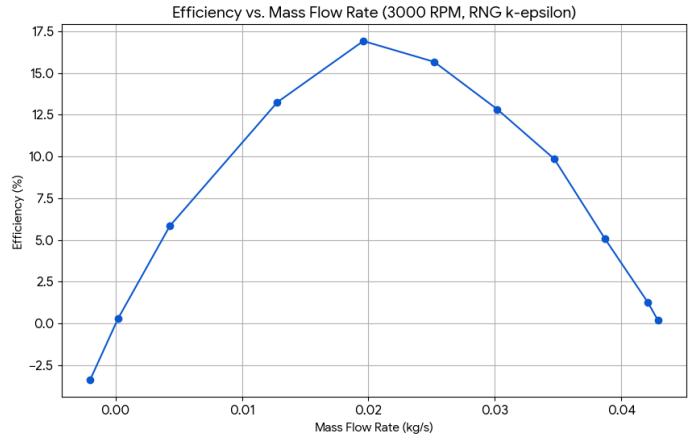

Figure 33. Efficiency vs Mass Flow Rate of the Base model at 3000 RPM (RNG k-Ɛ)

In Figure 33, the BEP is found at around 2500 Pa BC, where flow rate is ~0.0196 kg/s (~1.15 LPM) and peak efficiency reaches ~16.91%. This is slightly lower than the SST k-ω model at the same RPM, which recorded a peak efficiency of ~17.62% at ~0.0204 kg/s (~1.49 LPM). The RNG model predicts marginally lower efficiency.

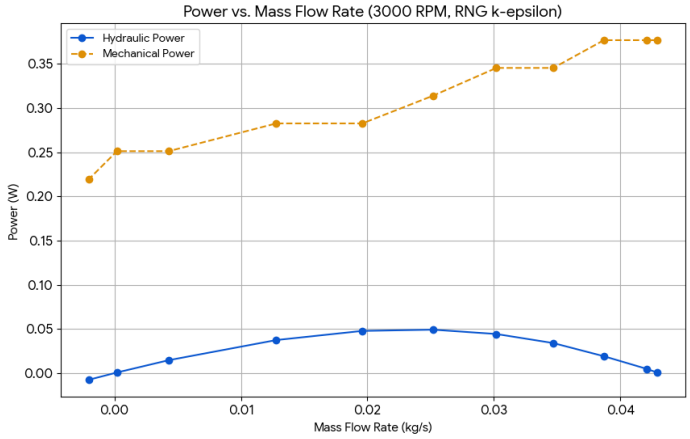

Figure 34. Power vs Mass Flow Rate of the Base model at 3000 RPM (RNG k-Ɛ)

The power curve (Figure 34) follows the same rising mechanical power trend as SST k-ω. However, hydraulic power levels off earlier due to earlier flow reversal, indicating the RNG model's sensitivity to adverse pressure gradients and swirl under these conditions.

6.3 Comparison of Turbulence Models (SST k-omega vs. RNG k-epsilon at 3000 RPM)

A comparative analysis of the head and efficiency curves between the SST k-omega and RNG k-epsilon turbulence models at 3000 RPM highlighted the subtle differences in their predictions of flow behavior and pump performance.

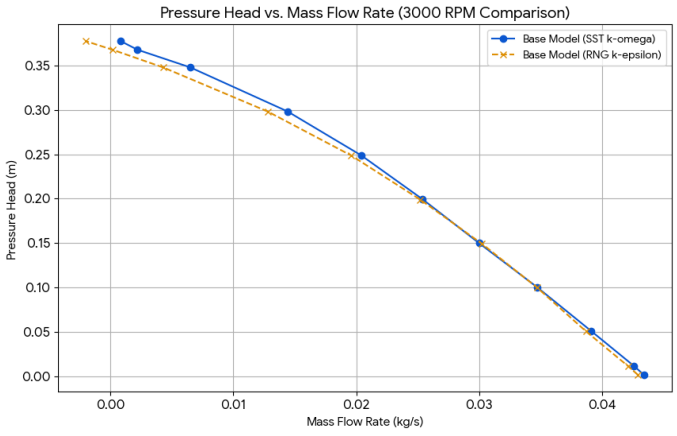

Figure 35. Pressure Head vs Mass Flow Rate of base model comparing two turbulence models

Head vs. Flow Rate (Figure 35):

- Both models exhibit a nearly identical trend in pressure head, confirming qualitative agreement.
- However, SST k-ω generally maintains marginally higher head across most of the operating range, whereas RNG k-ε may show slightly different behavior at the very onset of flow collapse. This could be attributed to the RNG model's enhanced swirl handling, making it slightly more optimistic in rotating flow regions, avoiding reverse flow [3].

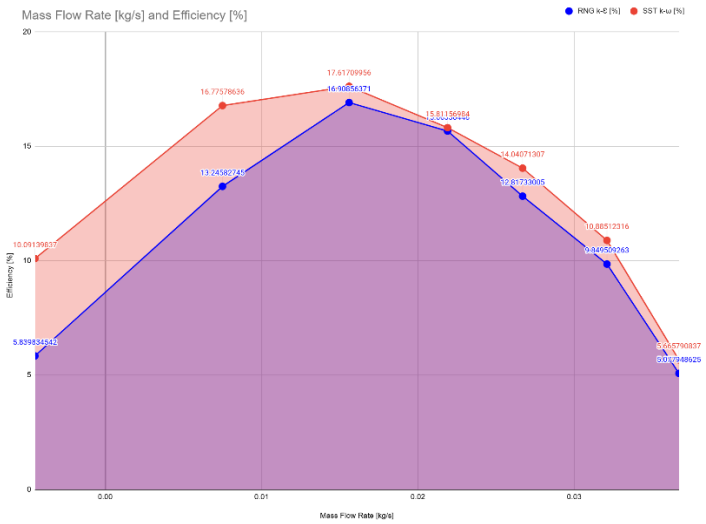

Figure 36. Efficiency vs Mass Flow Rate of base model comparing two turbulence models

Efficiency vs. Flow Rate (Figure 36):

- The SST k-ω model shows a broader efficiency curve, with a peak efficiency of ~17.62% at ~0.0204 kg/s (1.49 LPM).
- The RNG k-ε model predicts a slightly lower peak efficiency of ~16.91% but at a lower flow rate of ~0.0196 kg/s (1.15 LPM), showing it reaches optimal performance earlier.
- Beyond the BEP, SST k-ω demonstrates a more gradual drop in efficiency, whereas RNG k-ε shows a sharper decline as it approaches the shut-off region.

These differences arise due to the nature of each turbulence model. SST k-ω blends the near-wall accuracy of the k-ω formulation with the free-stream robustness of k-ε, making it more stable and accurate for flows with adverse pressure gradients, common in blood pumps [26]. RNG k-ε includes additional terms for swirl and rapid strain rates, making it suitable for highly swirling flows but sometimes less stable near complex boundaries [27].

Thus, SST k-ω may be preferable for modeling near-wall shear stresses and long-term hemocompatibility, while RNG k-ε can complement analysis where core swirling structures dominate.

6.4 Comparative Analysis of Base Model vs. Modified Rotor Blade Model (SST k-omega)

The modifications to the rotor blades (narrowed by 20% and sharp edges rounded) have a visible impact on the internal flow characteristics. These changes primarily aim to optimize flow smoothness and potentially reduce blood damage, which is evident in

the contours.

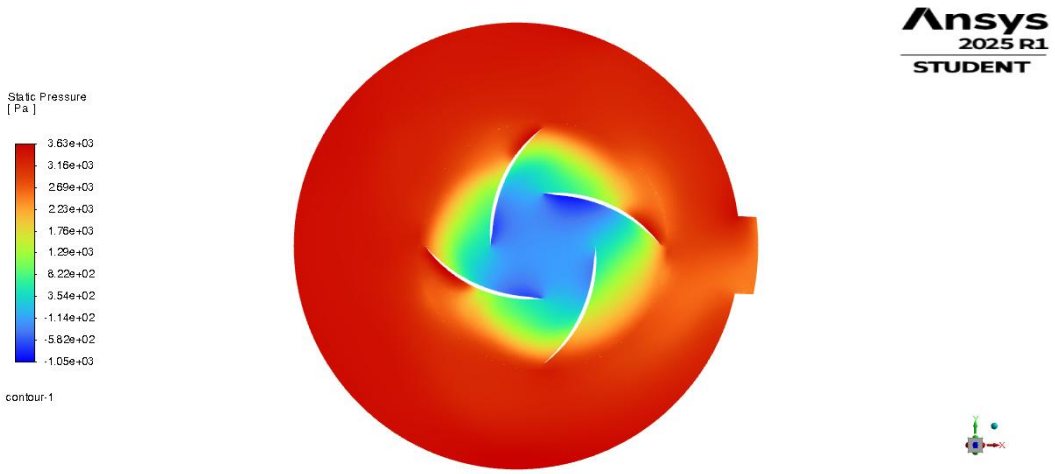

Figure 37. Pressure at Z-axis iso surface of Base Model (SST k-

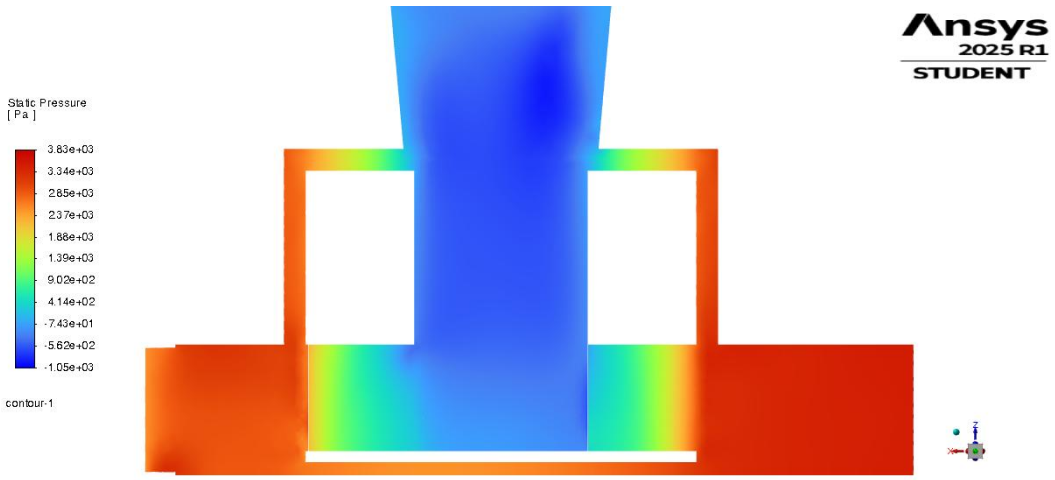

Figure 38. Pressure at Y-axis iso surface of Base Model (SST k- ω).

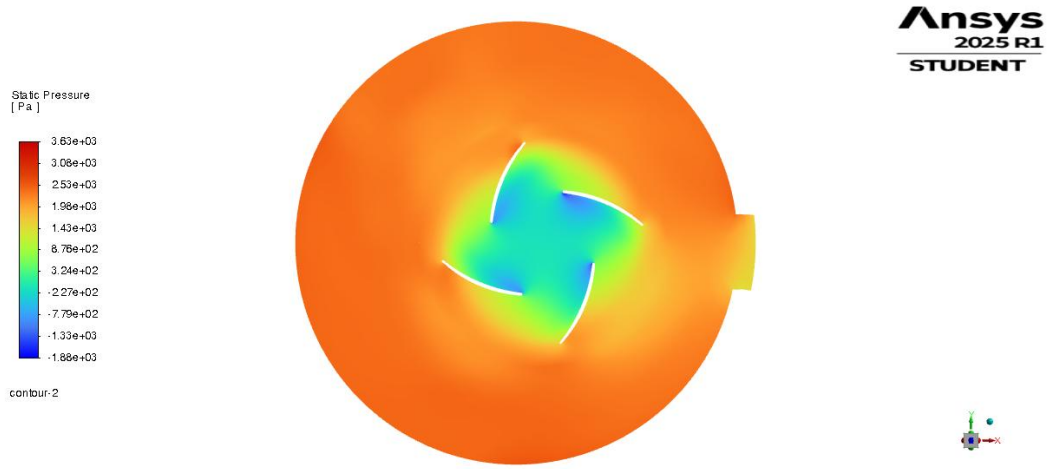

Figure 39. Pressure at Z-axis iso surface of Modified Rotor Blades Model (SST k- ω).

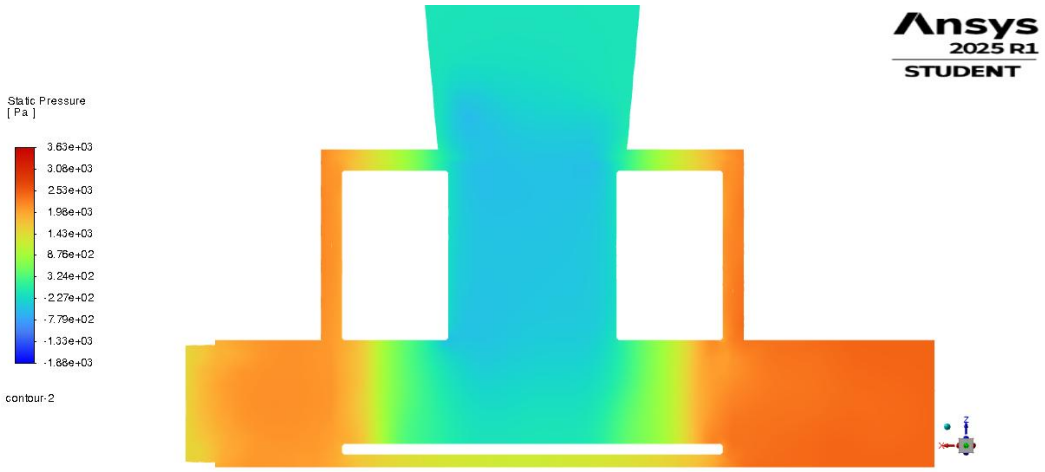

Figure 40. Pressure at Y-axis iso surface of Modified Rotor Blades Model (SST k- ω).

The pressure distribution within the pump was examined through top-down and side-view iso-surfaces along the Z and Y axes, respectively. In the base model, pressure contours clearly illustrate a gradual increase from the central inlet toward the outer casing, with peak pressure observed near the radial outlet. The region around the impeller blades shows well-defined pressure gradients, especially at the blade surfaces. In contrast, the modified blade model reveals a slightly smoother and more uniform pressure field. The reduced sharpness in pressure gradients near the blades suggests a more gradual pressure buildup, likely attributed to the rounded edges and narrowed blade profile, which facilitate less abrupt fluid-structure interaction. Side-view contours confirm similar axial-to-radial pressure transition in both models, indicating that the essential pumping mechanism remains intact despite geometric modifications (Figure 37, 38, 39, 40).

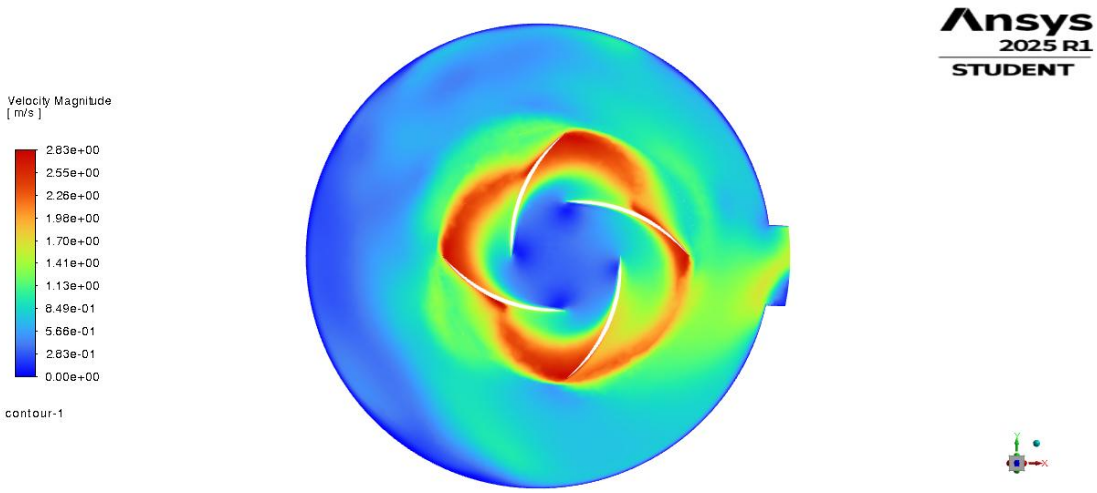

Figure 41. Velocity at Z-axis iso surface of Base Model (SST k- ω).

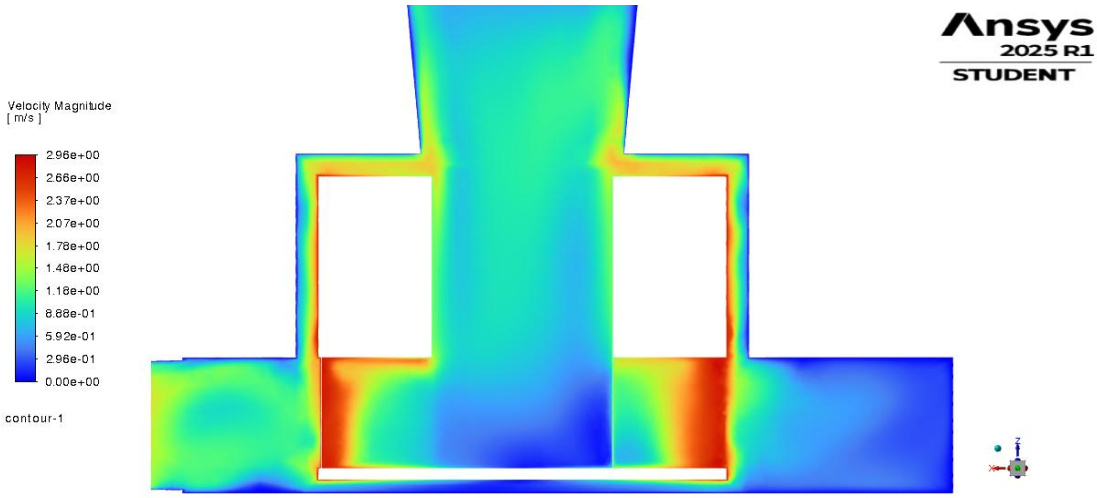

Figure 42. Velocity at Y-axis iso surface of Base Model (SST k- ω).

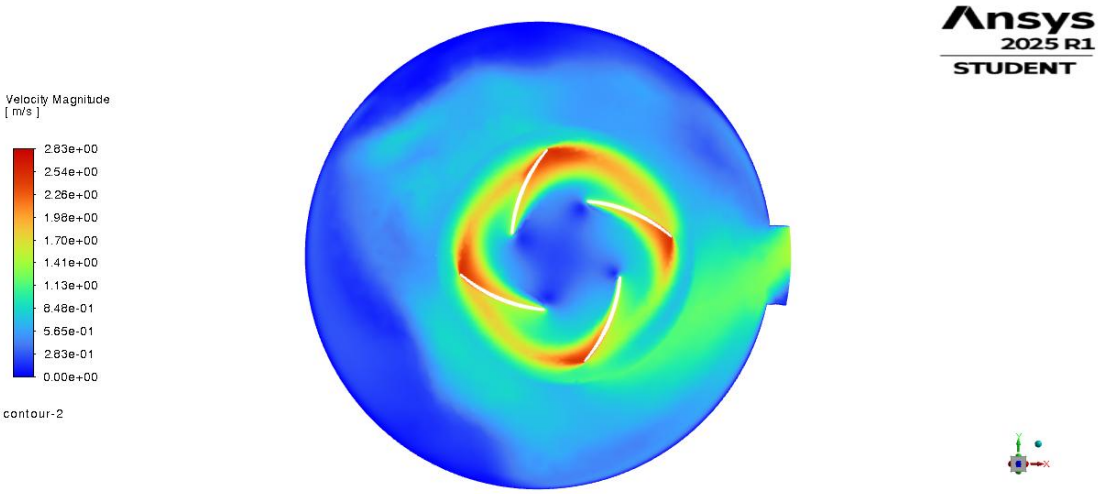

Figure 43. Velocity at Z-axis iso surface of Modified Rotor Blades Model (SST k- ω).

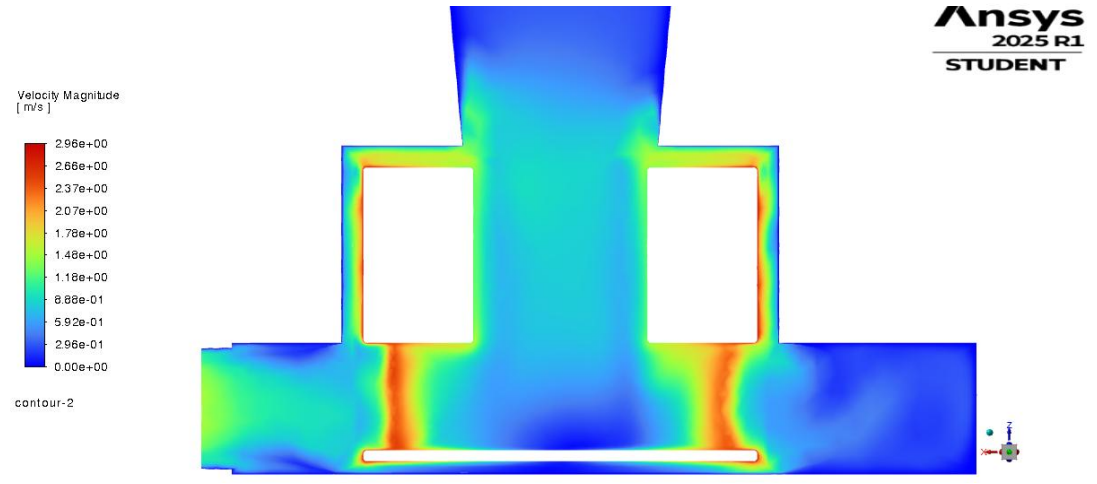

Figure 44. Velocity at Y-axis iso surface of Modified Rotor Blades Model (SST k- ω).

Velocity distribution was evaluated to assess the flow acceleration and potential recirculation zones. The base model displays concentrated high-velocity zones at the

impeller blade tips and along the primary radial flow path. Some minor regions of turbulence and mixing are evident, particularly downstream of the impeller. The modified rotor blades, however, demonstrate a similar high-velocity pattern near the blades but with visibly smoother downstream flow. The narrower blade channels and reduced surface complexity appear to generate a more coherent velocity field, potentially improving volumetric efficiency and minimizing chaotic flow transitions. The side view supports this observation, showing largely unchanged axial-to-radial acceleration while hinting at improved directional flow consistency in the modified model (Figure 41, 42, 43, 44).

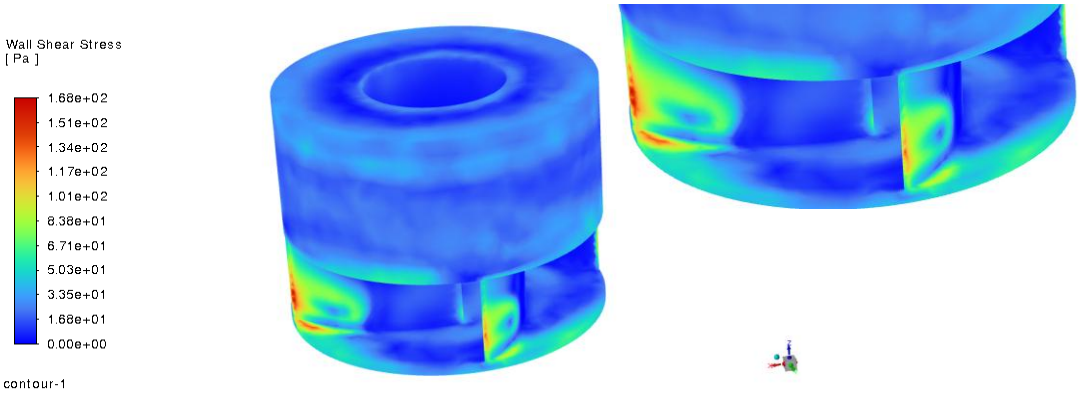

Figure 45. Wall Shear Stress at the Rotor Walls of the Base Model (SST k- ω).

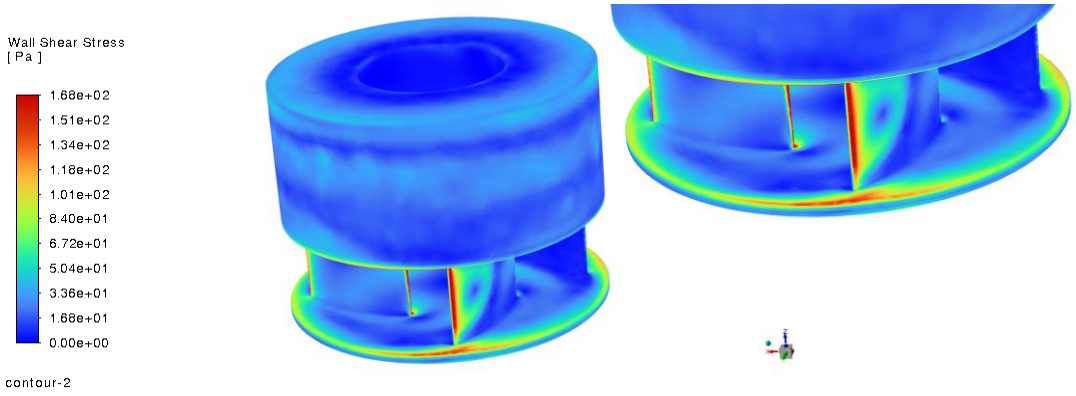

Figure 46. Wall Shear Stress at the Rotor Walls of the Modified Rotor Blades model (SST k- ω).

The modified design aimed to enhance efficiency by reducing both pressure and overall shear stress for improved hemocompatibility. While the target pressure reduction was achieved, the Wall Shear Stress (WSS) analysis, crucial for evaluating hemocompatibility, reveals a more nuanced outcome. In the base model, WSS was notably concentrated at the blade leading/trailing edges and the rotor-housing interface, with values peaking around 168 Pa across larger blade areas. Conversely, the modified blade model exhibits a visibly more distributed and subdued WSS field over its newly rounded blade surfaces.

However, it also introduced new, highly localized areas where WSS still peaked at around 168 Pa. Given that the original design had shear stress spread over broader regions, it is inconclusive to definitively state whether this modified design represents an overall improvement or inadvertently worsened hemocompatibility due to these concentrated new peaks (Figure 45) and (Figure 46).

A comparative analysis of the head and efficiency curves between the Base model and the model with the modified blades design at 3000 RPM with SST k-omega turbulence model, highlighted the significant differences in their predictions of flow behavior and pump performance.

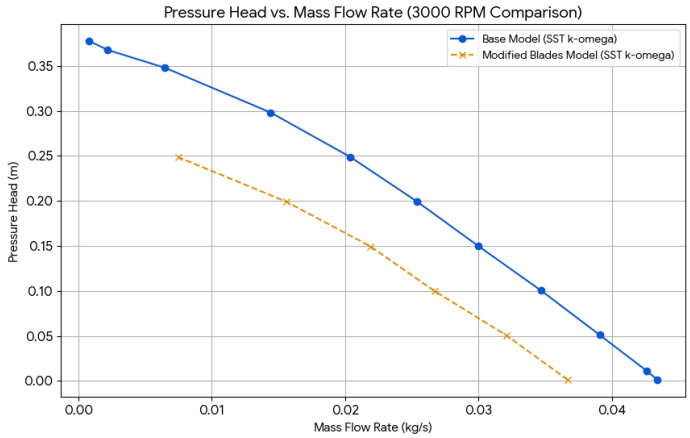

Figure 47. Pressure Head vs Mass Flow Rate of our model at two different modified designs (SST k-ω)

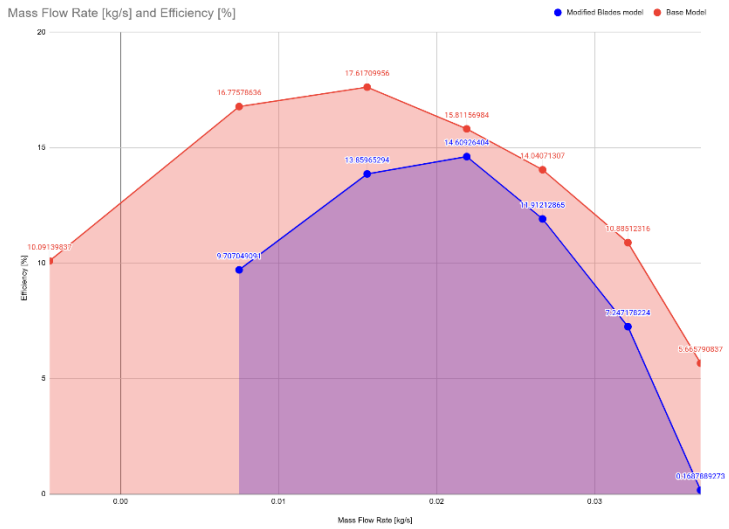

Figure 48. Efficiency vs Mass Flow Rate of our model at two different modified designs (SST k-ω)

The modified rotor blades were designed to assess how a smoother and narrower blade profile would influence pump performance. These changes aim to reduce local turbulence and improve flow guidance, especially at lower flow rates.

- Head vs. Flow Rate (Figure 47): The curve shows a notable reduction in pressure head compared to the base model, particularly at higher outlet pressures. Although the trend looks the same, the max head remains at 0.24 m while it's counterpart at the same RPMs generate a max Head of 0.37 m.
- Efficiency vs. Flow Rate (Figure 48): The peak efficiency is reached at 1500 Pa BC, where the flow rate is ~0.0219 kg/s and efficiency ~14.61%. This is slightly lower than the base model at 3000 RPM (15.81%) but at a similar flow rate. This suggests that while smoother blades help sustain flow, they slightly reduce the total work done on the fluid.
- Hydraulic power increases up to the BEP and then declines, while mechanical power continues to rise due to increasing torque. Compared to the base model, the modified blade version maintains slightly lower torque requirements, likely due to reduced flow resistance across the impeller.
- Flow Reversal was observed beyond 3000 Pa BC, with a negative mass flow rate appearing at 3000 Pa BC and higher, indicating a lower shut-off pressure tolerance than the base design.

6.5 Comparison with Published Data (Abbott's HeartMate III Curve)

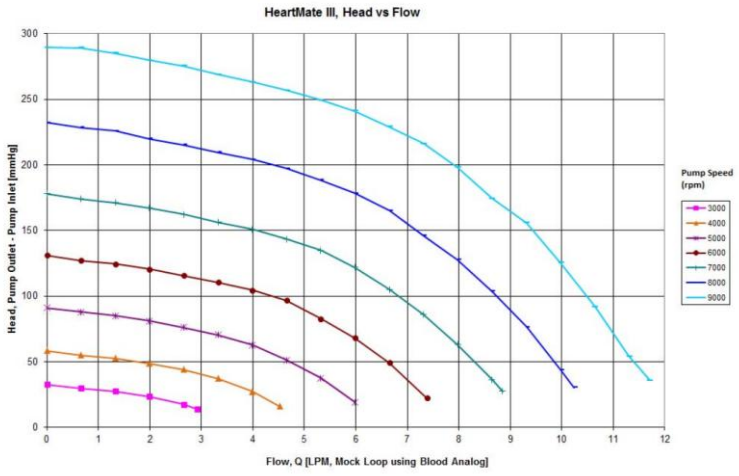

Figure 49. Pressure vs Mass Flow Rate of HeartMate 3 at different RPMs, by Abbott [21]

On the documentation provided by Abbott (Figure 49) [21], we find an official pump performance curve for the HeartMate 3, issued by the company. Since our simulations have already produced values for pressure head (H, in meters) and mass flow rate (ṁ, in

kg/s), we can now compare our simulation data to the official curve for different rotational speeds (RPMs). This comparison will help validate the fidelity of our CFD model. Before plotting and comparing the results, we need to convert:

- Pressure Head from meters (m) to millimeters of mercury (mmHg)
- Mass Flow Rate from kg/s to liters per minute (L/min)

The following conversion formulas will be used:

Pressure Head Conversion (from meters to mmHg):

Pressure Head [mmHg] = (Pressure Head [m] × 1025 × 9.81) / 133.322

Where:

- 1025 = Density of blood in kg/m³
- 9.81 = Acceleration due to gravity in m/s²
- 133.322 = Conversion factor from Pascal to mmHg

Mass Flow Rate Conversion (from kg/s to L/min):

Mass Flow Rate [LPM] = (Mass Flow Rate [kg/s] / 1025) × 60000

Where:

- 1025 = Density of blood in kg/m³
- 60000 = Conversion factor (1 m³/s = 60000 L/min)

Once these conversions are applied, we can overlay our simulation results on the manufacturer's performance curve to assess accuracy and simulate fidelity for each RPM. This step is essential in validating the CFD model and determining how closely it replicates real-world performance of the HeartMate 3 device.

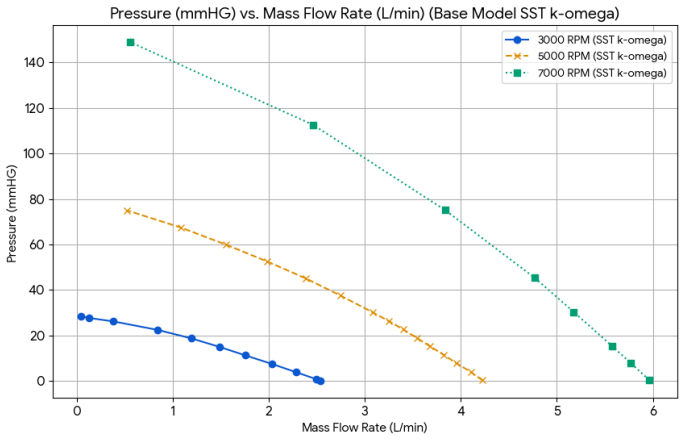

Figure 50. Pressure vs Mass Flow Rate of our model at different RPMs.

The simulated performance curves for the HeartMate 3-inspired model (Figure 50) show notable alignment with the manufacturer-provided graph from Abbott (Figure 49), especially at lower mass flow rates. For the tested rotational speeds of 3000, 5000, and 7000 RPM, the pressure head values closely follow the trends of the official data in the regions where flow rate is low.

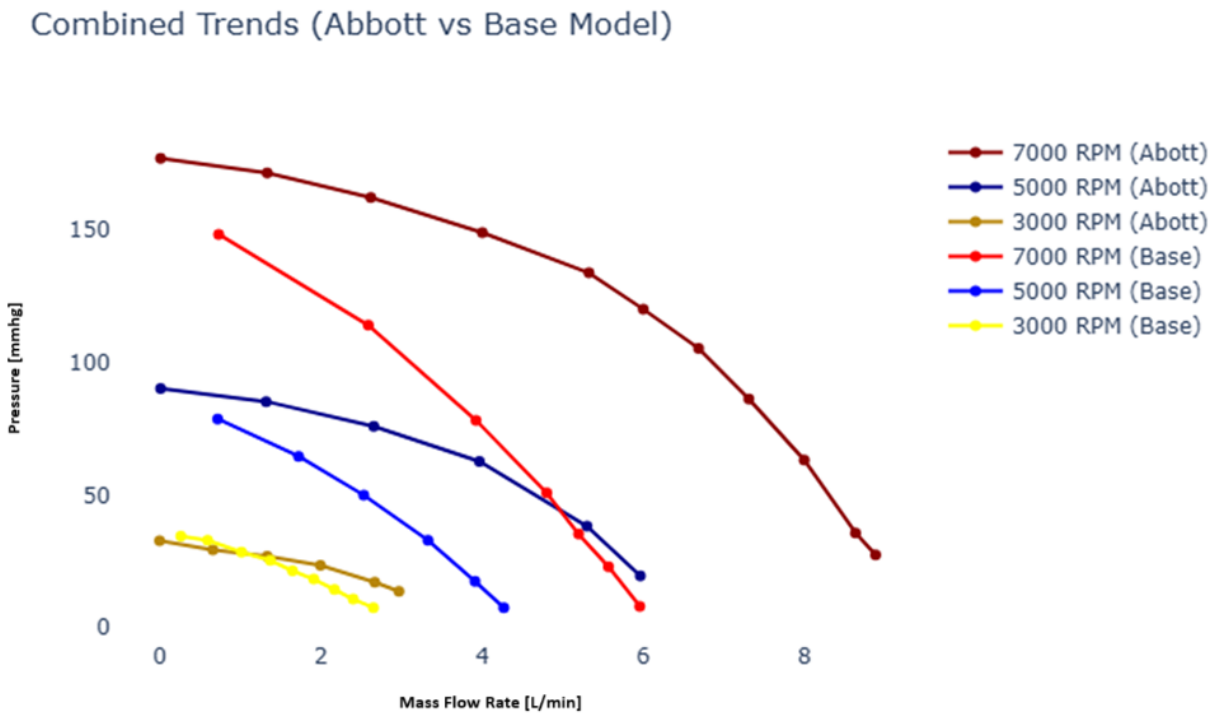

Figure 51. Cobined plot of H-Q curve comparing the Base Model and Abbott documentation.

However, as the flow rate increases, deviations become more apparent (Figure 51). For example, at 3000 RPM, the simulated curve matches Abbott's data well when flow exceeds ~3 L/min, but drops off rapidly below this point. In contrast, the manufacturer's curve maintains a higher-pressure head even at higher flow rates. This divergence becomes more pronounced at higher RPMs. These discrepancies likely stem from a combination of factors:

- Design simplifications in geometry due to the proprietary nature of HeartMate 3
- Approximated internal dimensions and blade profiles
- Mesh quality constraints, especially at curved or small-scale features
- Modeling blood as a Newtonian fluid, which may overlook key non-Newtonian effects at lower shear rates

Despite these limitations, the CFD model captures the overall performance trend of the pump reasonably well and supports its utility for comparative and design-iteration studies.
Analysis of Specific Flow Phenomena (WSS, Recirculation, etc.)

7 Conclusion

7.1 Summary of Findings

This study successfully developed and validated a computational fluid dynamics (CFD) model that hydraulically represents the performance characteristics of the HeartMate 3 ventricular assist device (VAD). The simulations captured key hydraulic behavior across varying RPMs, under multiple outlet pressure conditions, using two turbulence models (SST k-ω and RNG k-ε), and evaluated both a base impeller design and a modified blade geometry.

At 3000 RPM, the base model (SST k-ω) reached a Best Efficiency Point (BEP) at approximately 0.0204 kg/s (1.49 L/min), with a maximum efficiency of 17.6% and a shut-off head of 3776 Pa (28.48 mmHg). At 5000 RPM, the BEP was identified between 0.0408 and 0.0265 kg/s, with a peak efficiency of 18.44% at 7000 Pa, confirming increased performance capacity at higher speeds. At 7000 RPM, the model achieved its highest overall efficiency of 20.02% at 15000 Pa, with the shut-off limit occurring around 20000 Pa.

Comparing turbulence models at 3000 RPM, both SST k-ω and RNG k-ε predicted similar flow-efficiency trends. However, SST k-ω consistently provided slightly higher peak efficiency and more stable convergence, especially near wall boundaries, supporting its suitability for rotating blood pump simulations. RNG k-ε, while effective, demonstrated a sharper efficiency drop near reverse flow and greater sensitivity to outlet pressure changes.

The blade-modified model (SST k-ω) showed improved performance in specific conditions, delivering comparable flow rates at slightly lower torque requirements. It exhibited a modest reduction in peak head and an earlier reverse flow onset. Crucially, WSS analysis revealed a nuanced outcome regarding hemocompatibility. While the base model displayed prominent, concentrated WSS hot spots near blade edges and the rotor-housing interface, reaching peaks around 168 Pa across larger blade areas, the modified blade model exhibited a visibly more distributed and subdued WSS field over its newly rounded blade surfaces. However, it also introduced new, highly localized areas where WSS still peaked at around 168 Pa. Given that the original design had shear stress spread over broader regions, it is inconclusive to definitively state whether this modified design represents an overall improvement or inadvertently worsened hemocompatibility due to these concentrated new peaks. This indicates a design trade-off: improved flow smoothness at the cost of reduced pressure generation, with complex implications for shear-induced blood damage.

When compared to the manufacturer-provided HeartMate 3 performance curve [21], the CFD-predicted trends showed high similarity at lower flow rates, particularly in the 3000–5000 RPM range. Some deviations at low flow rates and extreme pressure conditions were attributed to necessary design simplifications and modeling assumptions.

7.2 Efficiency, BEP, and Operational Insights

The identification of Best Efficiency Points (BEP) across all tested RPMs holds critical importance for clinical VAD operation. Operating a centrifugal blood pump at or near its BEP ensures Maximal hydraulic output with minimal mechanical input, thereby improving energy efficiency and extending battery life and Reduced internal recirculation and turbulence, which are key contributors to blood damage and hemolysis.

Each efficiency curve clearly displayed a sharp drop beyond the BEP, emphasizing the need to avoid operation in under-loaded (low flow) conditions. Reverse flow, particularly around 3700–4000 Pa at 3000 RPM, was consistently observed as a stability threshold, marking the maximum head the pump can sustain before flow deteriorates.

7.3 Internal Flow Characteristics

Contour visualizations of pressure, velocity, and wall shear stress (WSS) further validated the hydrodynamic behavior of the modeled VAD and revealed the impact of blade modifications. Pressure contours confirmed expected axial-to-radial pressure gradients, with the modified blades promoting slightly smoother pressure distribution due to their narrowed and rounded profile. Velocity contours showed high-speed flow regions around the impeller tips in both models, but the modified rotor produced more coherent downstream flow, suggesting improved volumetric efficiency. The WSS contours highlighted a reduction in peak shear stress concentrations on the modified blade surfaces, despite a higher maximum value, the stress was distributed more evenly. This result supports the hypothesis that smoother blade geometry may improve hemocompatibility by reducing localized stress zones responsible for blood damage. These findings emphasize the importance of internal flow structure in assessing VAD performance beyond global hydraulic metrics.

7.4 Limitations of the Study

To ensure academic integrity, several limitations of this study must be acknowledged:

1. Newtonian Fluid Assumption: Blood was modeled as a Newtonian fluid with constant viscosity throughout the simulations. While this simplification was adopted to streamline computational efforts and is often considered acceptable for the high-shear environments prevalent in rotary blood pumps, it can lead to subtle changes in the prediction of local flow dynamics. Specifically, the non-Newtonian shear-thinning behavior of blood, which becomes more pronounced in low-shear

or recirculation zones, is not fully captured. This limitation could affect the precise quantification of near-wall shear stress and, consequently, the assessment of blood damage [14], [20].
2. Steady-State Flow: The simulations were performed in steady-state. However, blood flow in the human body is inherently pulsatile. A transient simulation with a pulsatile inlet profile could better emulate cardiac cycles and shear stress dynamics.
3. Simplified Geometry: The HeartMate 3's actual internal geometry is proprietary. The model used here was constructed from approximate and published profiles. While hydraulically representative, this simplification may influence recirculation zones and hemolysis prior zone detection difficult.

8 References

1. Crone, V., Knüppel, F., Hahne, M., et al. (2024). Dynamic VAD simulations: Performing accurate simulations of ventricular assist devices in interaction with the cardiovascular system. The International Journal of Artificial Organs, 47(8), 624-632.
2. Doost, S.N., Zhong, L., & Morsi, Y.S. (2017). Ventricular assist devices: current state and challenges. Journal of Medical Devices, 11(4), 040801.
3. Fraser, K.H., Taskin, M.E., Griffith, B.P., & Wu, Z.J. (2011). The use of computational fluid dynamics in the development of ventricular assist devices. Medical Engineering & Physics, 33(3), 263-280.
4. Goodreau, M. & Arensman, D. (2018, May). Tips and Tricks for Accurately Modeling Pumps. In PSIG Annual Meeting (pp. PSIG-1818). PSIG.
5. Jaiswal, N.P. (2014). CFD analysis of centrifugal pump: a review. Journal of Engineering Research and Applications, 4, 175-178.
6. Karassik, I.J. (2001). Pump Handbook.
7. Maher, T.R., Butler, K.C., Poirier, V.L., & Gernes, D.B. (2001). HeartMate left ventricular assist devices: A multigeneration of implanted blood pumps. Artificial Organs, 25(5), 422-426.
8. Menon, E.S. (2009). Working Guide to Pump and Pumping Stations: Calculations and Simulations. Gulf Professional Publishing.
9. Salerno, C.T., Hayward, C., Hall, S., Goldstein, D., Saeed, D., Schmitto, J., ... & Pagani, F.D. (2022). HVAD to HeartMate 3 left ventricular assist device exchange: best practices recommendations. European Journal of Cardio-Thoracic Surgery, 62(1), ezac169.
10. Soucy, K.G., Koenig, S.C., Giridharan, G.A., Sobieski, M.A., & Slaughter, M.S. (2013). Rotary pumps and diminished pulsatility: Do we need a pulse? ASAIO Journal, 59(4), 355-366.

11. Timms, D. (2011). A review of clinical ventricular assist devices. Medical Engineering & Physics, 33(9), 1041-1047.
12. Westaby, S. & Frazier, O.H. (2012). Long-term biventricular support with rotary blood pumps: Prospects and pitfalls. European Journal of Cardio-Thoracic Surgery, 42(2), 203-208.
13. Zawawi, M.H., Saleha, A., Salwa, A., Hassan, N.H., Zahari, N.M., Ramli, M.Z., & Muda, Z.C. (2018, November). A review: Fundamentals of computational fluid dynamics (CFD). In AIP Conference Proceedings (Vol. 2030, No. 1). AIP Publishing.
14. Nader E, Skinner S, Romana M, Fort R, Lemonne N, Guillot N, Gauthier A, Antoine-Jonville S, Renoux C, Hardy-Dessources MD, Stauffer E, Joly P, Bertrand Y, Connes P. Blood Rheology: Key Parameters, Impact on Blood Flow, Role in Sickle Cell Disease and Effects of Exercise. Front Physiol. 2019 Oct 17;10:1329. doi: 10.3389/fphys.2019.01329. PMID: 31749708; PMCID: PMC6842957.
15. "Human Blood – an Overview." *ScienceDirect*, https://www.sciencedirect.com/topics/engineering/human-blood. Accessed 30 May 2025.
16. Vandenberge, John, et al. "In Vitro Comparison of Device-Induced Hemolysis, Platelet Defects, and von Willebrand Factor Degradation Between the HeartMate 2 and HeartMate 3 Pumps." *Artificial Organs* (2025).
17. *I Heartmate 3TM Left Ventricular Assist Device*, www.cardiovascular.abbott/content/dam/cv/cardiovascular/hcp/education-training/heart-failure/documents/hf-heartmate3-lvad-pump-parameters.pdf. Accessed 1 June 2025.
18. Mark, N. and Lawson , E.C. (no date) *Llusurgery*, *LEFT VENTRICULAR ASSIST DEVICES.* (Accessed: 01 June 2025).
19. Belkin, Mark N., et al. "Physiology and clinical utility of HeartMate pump parameters." *Journal of cardiac failure* 28.5 (2022): 845-862.
20. Jung, Jonghwun, and Ahmed Hassanein. "Three-phase CFD analytical modeling of blood flow." *Medical engineering & physics* 30.1 (2008): 91-103.
21. Thoratec Corporation. (2017). *HEART MATE 3 LEFT VENTRICULAR ASSIST SYSTEM INSTRUCTIONS FOR USE*.
22. World Health Organization. (2021). *Cardiovascular diseases (CVDs)*. Retrieved from https://www.who.int/news-room/fact-sheets/detail/cardiovascular-diseases-(cvds)
23. Slaughter, M. S., Pagani, F. D., Rogers, J. G., et al. (2009). Clinical management of continuous-flow left ventricular assist devices in advanced heart failure. *The Journal of Heart and Lung Transplantation*, 28(4), 326–336.
24. Fraser, K. H., Zhang, T., Taskin, M. E., Griffith, B. P., & Wu, Z. J. (2011). A quantitative comparison of mechanical blood damage parameters in rotary ventricular assist devices: CFD predictions. *ASAIO Journal*, 57(4), 330–337.
25. Taylor, C. A., Figueroa, C. A. (2009). Patient-specific modeling of cardiovascular mechanics. *Annual Review of Biomedical Engineering*, 11, 109–134.

26. Mehra, M. R., Goldstein, D. J., Uriel, N., et al. (2018). Two-year outcomes with a magnetically levitated cardiac pump in heart failure. *New England Journal of Medicine*, 378(15), 1386–1395.
27. Kirklin, J. K., Pagani, F. D., Kormos, R. L., et al. (2017). Eighth INTERMACS annual report: Special focus on framing the impact of adverse events. *The Journal of Heart and Lung Transplantation*, 36(10), 1080–1086.
28. Netuka, I., Ivák, P., Sood, P., et al. (2018). Biocompatibility and stability of a fully magnetically levitated circulatory pump. *The Journal of Heart and Lung Transplantation*, 37(3), 283–290.
29. Wu, J., Zeng, P., Wang, S., et al. (2018). Numerical simulation and performance evaluation of a novel axial flow blood pump with a magnetic suspension system. *Medical & Biological Engineering & Computing*, 56(9), 1613–1625.
30. Morris, P. D., Narracott, A., von Tengg-Kobligk, H., et al. (2016). Computational fluid dynamics modelling in cardiovascular medicine. *Heart*, 102(1), 18–28.
31. Nobili, M., Sheriff, J., Morbiducci, U., Redaelli, A., & Bluestein, D. (2008). Platelet activation due to hemodynamic shear stresses: Damage accumulation model and comparison to in vitro measurements. *ASAIO Journal*, 54(1), 64–72.
32. Garon, A., & Farinas, M. I. (2004). Fast three-dimensional numerical modeling of shear stress distributions on blood cells. *Annals of Biomedical Engineering*, 32(12), 1691–1699.
33. Giersiepen, M., Wurzinger, L. J., Opitz, R., & Reul, H. (1990). Estimation of shear stress-related blood damage in heart valve prostheses—In vitro comparison of 25 aortic valves. *International Journal of Artificial Organs*, 13(5), 300–306.
34. Paul, R., Apel, J., Klaus, S., et al. (2003). Shear stress-related blood damage in laminar couette flow. *Artificial Organs*, 27(6), 517–529.
35. Cho, Y. I., & Kensey, K. R. (1991). Effects of the non-Newtonian viscosity of blood on flows in a diseased arterial vessel. *Part 1: Steady flows*. *Biorheology*, 28(3–4), 241–262.
36. Sato, Y., Kunugi, T., & Wang, L. (2018). Comparison of numerical stability in turbulent flow simulations using k–ε, k–ω, and k–σ models. *Journal of Thermal Science*, 27(4), 315–327.
37. Boughner, D. R., et al. (2013). Numerical modeling of turbulence effects in the flow of a ventricular assist device. *IEEE Transactions on Biomedical Engineering*, 60(11), 3125–3133.
38. Zhang, J., Griffith, B. P., Wu, Z. J. (2021). Computational fluid dynamics-based evaluation of blood pump hemocompatibility. *Artificial Organs*, 45(4), 400–414.
39. Islam, M., Ikegami, Y., & Takahashi, S. (2019). Design optimization of a blood pump impeller using computational fluid dynamics and genetic algorithms. *Journal of Biomechanics*, 84, 137–145.
40. Sharma, A., et al. (2020). CFD and experimental study of an axial blood pump with improved blade design. *Medical Engineering & Physics*, 77, 28–36.
41. Pope, S. B. (2000). *Turbulent Flows*. Cambridge University Press.
42. Wilcox, D. C. (2006). *Turbulence Modeling for CFD*. DCW Industries.
43. Menter, F. R. (1994). “Two-equation eddy-viscosity turbulence models for engineering applications.” *AIAA Journal*, 32(8), 1598–1605.

44. Yakhot, V., & Orszag, S. A. (1986). “Renormalization group analysis of turbulence. I. Basic theory.” *Journal of Scientific Computing*, 1(1), 3–51.
45. Versteeg, H. K., & Malalasekera, W. (2007). *An Introduction to Computational Fluid Dynamics: The Finite Volume Method*. Pearson Education.
46. White, F. M. (2011). *Fluid Mechanics* (7th ed.). McGraw-Hill Education.
47. Cengel, Y. A., & Cimbala, J. M. (2013). *Fluid Mechanics: Fundamentals and Applications* (3rd ed.). McGraw-Hill Education.
48. ANSYS Inc. (2024). *ANSYS Fluent Theory Guide 2024 R1*.
49. ANSYS Inc. (2024). *ANSYS Fluent User’s Guide 2024 R1*.
50. Li, L., Zhang, X., & Xu, G. (2017). “CFD study on performance prediction and optimization of a blood pump impeller.” *Journal of Mechanical Science and Technology*, 31(12), 5941–5950.
51. *What the heart does*. (n.d.). Edwards Lifesciences. https://www.edwards.com/gb/patients-care-partners/heart-valve-disease-information/what-the-heart-does
52. Patel, V. (2022, August 1). Centrifugal pump curves - 4 types of performance curves. HardHat Engineer. https://hardhatengineer.com/centrifugal-pump-curves/
53. Sivathasan, C. (2020). Chugging to silent machines: development of mechanical cardiac support. Indian Journal of Thoracic and Cardiovascular Surgery, 36(S2), 234–246. https://doi.org/10.1007/s12055-020-01010-2
54. Papathanasopoulou, Panorea, et al. "MRI measurement of time-resolved wall shear stress vectors in a carotid bifurcation model, and comparison with CFD predictions." Journal of Magnetic Resonance Imaging 17.2 (2003): 153-162.
55. Tyfa, Zbigniew, et al. "Influence of fluid rheology on blood flow haemodynamics in patient-specific arterial networks of varied complexity-in-silico studies." acta mechanica et automatica 18.1 (2024).

9 Appendices

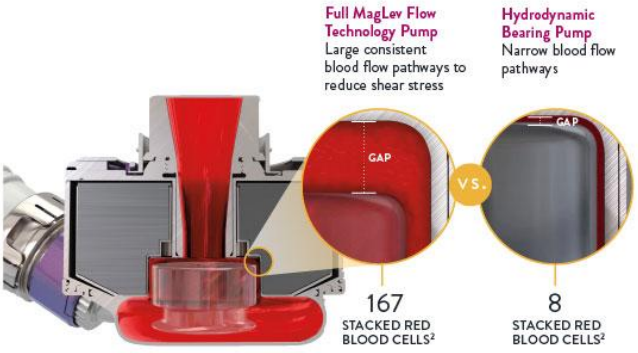

Figure 52. Inside design showing the gaps between the rotor and the stator [17]

Table 1. Metrics comparison of the Base model at 3000 RPM (SST k-omega)

3000 RPM										
Outlet Pressure BC (Pa)	**Outlet Pressure (Pa)**	**Inlet Pressure (Pa)**	**Mass Flow Rate (kg/s)**	**Torque (Nm)**	**ΔP (Pa)**	**Head (m)**	**Hydraulic Power (W)**	**Angular Velocity (rad/s)**	**Mechanical Power (W)**	**Efficiency (%)**
0	-7.66	-23.34	0.0434	0.0012	15.68	0.00156	0.00066	314	0.3768	0.18
100	92.44	-22.53	0.0426	0.0012	114.96	0.01143	0.00478	314	0.3768	1.27
500	493.83	-19.19	0.0391	0.0011	513.01	0.05102	0.01957	314	0.3454	5.67
1000	994.35	-15.27	0.0347	0.0010	1009.62	0.10041	0.03418	314	0.314	10.89
1500	1494.86	-11.47	0.0300	0.0010	1506.33	0.14981	0.04409	314	0.314	14.04
2000	1995.36	-8.16	0.0254	0.0010	2003.53	0.19925	0.04965	314	0.314	15.81
2500	2496.30	-5.19	0.0204	0.0009	2501.50	0.24878	0.04979	314	0.2826	17.62
3000	2996.96	-2.64	0.0144	0.0008	2999.60	0.29831	0.04214	314	0.2512	16.78
3500	3497.13	-0.63	0.0065	0.0007	3497.76	0.34785	0.02218	314	0.2198	10.09
3700	3697.61	-0.08	0.0022	0.0007	3697.69	0.36774	0.00794	314	0.2198	3.61
3800	3797.50	-0.03	0.0008	0.0007	3797.53	0.37767	0.00296	314	0.2198	1.35

Table 2. Metrics comparison of the Base model at 5000 RPM (SST k-omega)

5000 RPM										
Outlet Pressure BC (Pa)	**Outlet Pressure (Pa)**	**Inlet Pressure (Pa)**	**Mass Flow Rate (kg/s)**	**Torque (Nm)**	**ΔP (Pa)**	**Head (m)**	**Hydraulic Power (W)**	**Angular Velocity (rad/s)**	**Mechanical Power (W)**	**Efficiency (%)**
0	-25.52	-65.82	0.0722	0.0030	40.30	0.00401	0.00284	523.33	1.5700	0.18
500	475.85	-61.78	0.0701	0.0029	537.63	0.05347	0.03677	523.33	1.5177	2.42
1000	976.67	-57.52	0.0676	0.0028	1034.20	0.10285	0.06821	523.33	1.4653	4.65

5000 RPM										
Outlet Pressure BC (Pa)	**Outlet Pressure (Pa)**	**Inlet Pressure (Pa)**	**Mass Flow Rate (kg/s)**	**Torque (Nm)**	**ΔP (Pa)**	**Head (m)**	**Hydraulic Power (W)**	**Angular Velocity (rad/s)**	**Mechanical Power (W)**	**Efficiency (%)**
1500	1478.36	-53.47	0.0653	0.0028	1531.83	0.15234	0.09759	523.33	1.4653	6.66
2000	1980.02	-49.63	0.0629	0.0028	2029.65	0.20185	0.12455	523.33	1.4653	8.50
2500	2480.91	-45.85	0.0605	0.0027	2526.76	0.25129	0.14914	523.33	1.4130	10.55
3000	2981.59	-42.32	0.0581	0.0027	3023.90	0.30073	0.17140	523.33	1.4130	12.13
3500	3481.81	-38.57	0.0555	0.0026	3520.38	0.35010	0.19062	523.33	1.3607	14.01
4000	3983.48	-34.85	0.0527	0.0026	4018.33	0.39963	0.20660	523.33	1.3607	15.18
5000	4985.98	-27.73	0.0469	0.0026	5013.71	0.49862	0.22941	523.33	1.3607	16.86
6000	5986.51	-21.37	0.0408	0.0025	6007.88	0.59749	0.23914	523.33	1.3083	18.28
7000	6988.39	-15.26	0.0339	0.0024	7003.66	0.69652	0.23163	523.33	1.2560	18.44
8000	7989.73	-9.67	0.0265	0.0022	7999.39	0.79554	0.20681	523.33	1.1513	17.96
9000	8991.24	-4.72	0.0185	0.0021	8995.96	0.89465	0.16237	523.33	1.0990	14.77
10000	9993.01	-1.04	0.0090	0.0020	9994.05	0.99391	0.08775	523.33	1.0467	8.38

Table 3. Metrics comparison of the Base model at 7000 RPM (SST k-omega)

7000 RPM										
Outlet Pressure BC (Pa)	**Outlet Pressure (Pa)**	**Inlet Pressure (Pa)**	**Mass Flow Rate (kg/s)**	**Torque (Nm)**	**ΔP (Pa)**	**Head (m)**	**Hydraulic Power (W)**	**Angular Velocity (rad/s)**	**Mechanical Power (W)**	**Efficiency (%)**
0	-52.96	-128.81	0.10	0.006	75.85	0.00754	0.0075332	732.66	4.396	0.17
1000	950.1365	-120.02	0.09	0.0059	1070.16	0.10642	0.10283	732.66	4.3227	2.37
2000	1949.21	-111.61	0.09	0.0059	2060.82	0.20495	0.19140	732.66	4.3227	4.42
4000	3955.64	-95.66	0.0	0.0057	4051.31	0.40290	0.34940	732.66	4.1762	8.36

6000	5962.07	-80.52	0.08	0.0054	6042.60	0.60094	0.48046	732.66	3.9564	12.14
10000	9971.15	-52.16	0.06	0.0047	10023.31	0.99682	0.64051	732.66	3.4435	18.60
15000	14977.8	-22.68	0.04	0.0042	15000.57	1.49181	0.61612	732.66	3.0772	20.02
16000	15434.78	-12.54	0.03	0.0041	15447.33	1.53624	0.48376	732.66	3.0039	16.10
18000	18997.68	-5.65	0.01	0.0039	19003.34	1.88989	0.22433	732.66	2.8574	7.85
20000	19858.99	-1.05	0.00	0.0038	19860.05	1.97509	0.18406	732.66	2.7841	6.61

Table 4. Metrics comparison of the Base model at 3000 RPM (RNG k-epsilon)

3000 RPM										
Outlet Pressure BC (Pa)	**Outlet Pressure (Pa)**	**Inlet Pressure (Pa)**	**Mass Flow Rate (kg/s)**	**Torque (Nm)**	**ΔP (Pa)**	**Head (m)**	**Hydraulic Power (W)**	**Angular Velocity (rad/s)**	**Mechanical Power (W)**	**Efficiency (%)**
0	-6.19	-22.86	0.0429	0.0012	16.67	0.00166	0.00070	314.16	0.3768	0.19
100	93.93	-22.05	0.0421	0.0012	115.98	0.01153	0.00476	314.16	0.3768	1.26
500	488.17	-18.60	0.0387	0.0012	506.77	0.05040	0.01913	314.16	0.3768	5.08
1000	989.95	-14.97	0.0347	0.0011	1004.92	0.09994	0.03402	314.16	0.3454	9.85
1500	1491.15	-11.43	0.0302	0.0011	1502.58	0.14943	0.04427	314.16	0.3454	12.82
2000	1992.45	-8.04	0.0252	0.0010	2000.49	0.19895	0.04918	314.16	0.3140	15.66
2500	2493.93	-4.95	0.0196	0.0009	2498.89	0.24852	0.04778	314.16	0.2826	16.91
3000	2995.39	-2.15	0.0128	0.0009	2997.54	0.29811	0.03743	314.16	0.2826	13.25
3500	3496.54	-0.30	0.0043	0.0008	3496.84	0.34776	0.01467	314.16	0.2512	5.84
3700	3696.15	-0.02	0.0002	0.0008	3696.17	0.36759	0.00072	314.16	0.2512	0.29
3800	3795.18	0	-0.0020	0.0007	3795.18	0.37743	-0.00741	314.16	0.2198	-3.37

Table 5. Metrics comparison of the Modified Rotor Blade model at 3000 RPM (SST k-omega)

3000 RPM										
Outlet Pressure BC (Pa)	**Outlet Pressure (Pa)**	**Inlet Pressure (Pa)**	**Mass Flow Rate (kg/s)**	**Torque (Nm)**	**ΔP (Pa)**	**Head (m)**	**Hydraulic Power (W)**	**Angular Velocity (rad/s)**	**Mechanical Power (W)**	**Efficiency (%)**
0	-4.92	-16.76	0.0367	0.0008	11.84	0.00118	0.00042	314.16	0.2512	0.17
500	495.68	-12.96	0.0321	0.0007	508.65	0.05059	0.01593	314.16	0.2198	7.25
1000	996.17	-8.98	0.0267	0.0007	1005.15	0.09996	0.02618	314.16	0.2198	11.91
1500	1496.99	-5.93	0.0219	0.0007	1502.92	0.14947	0.03211	314.16	0.2198	14.61
2000	1998.50	-3.11	0.0156	0.0007	2001.61	0.19906	0.03046	314.16	0.2198	13.86
2500	2498.67	-0.70	0.0075	0.0006	2499.37	0.24856	0.01829	314.16	0.1884	9.71
3000	N/A	0	-0.0045	0.0005	—	—	—	314.16	0.1570	—